Periodic Plasmonic Nanoantennas in a Piecewise Homogeneous Background

by

Saba Siadat Mousavi

A thesis presented to the
Faculty of Graduate and Postdoctoral Studies
in partial fulfillment of the requirements for the degree of

Master of Applied Science
In Electrical Engineering

Ottawa-Carleton Institute for Electrical and Computer Engineering
School of Electrical Engineering and Computer Science
Faculty of Engineering
University of Ottawa

Abstract

Optical nanoantennas have raised much interest during the past decade for their vast potential in photonics applications. This thesis investigates the response of periodic arrays of nanomonopoles and nanodipoles on a silicon substrate, covered by water, to variations of antenna dimensions. These arrays are illuminated by a plane wave source located inside the silicon substrate. Modal analysis was performed and the mode in the nanoantennas was identified. By characterizing the properties of this mode certain response behaviours of the system were explained. Expressions are offered to predict approximately the resonant length of nanomonopoles and nanodipoles, by accounting for the fringing fields at the antenna ends and the effects of the gap in dipoles. These expressions enable one to predict the resonant length of nanomonopoles within 20% and nanodipoles within 10% error, which significantly facilitates the design of such antennas for specific applications.

Acknowledgments

First and foremost I wish to express my gratitude to my supervisors Dr. Pierre Berini and Dr. Derek McNamara for giving me the opportunity to be a part of this research, for their invaluable advice, and for their endless patience and encouragements. This work would not have been possible without their help and support.

I am deeply grateful to my family, specially my dearest parents, who made all this possible by their unconditional love and support.

I would like to thank all my friends and colleagues in our research group for providing such a fun and friendly environment.

Acronyms

ADD	Anti-bonding Dipole-Dipole mode
BDD	Bonding Dipole-Dipole mode
BEM	Boundary Element Method
BQD	Bonding Quadrupole-Dipole mode
DI	Dipole mode in bar
Dx	Dipole mode in cross
FDTD	Finite Difference Time Domain
FoM	Figure of Merit
FWHM	Full Width at Half Maximum
IR	Infrared
LSPR	Localized Surface Plasmon Resonance
Q factor	Quality factor
Qx	Quadrupole mode in cross
RI	Refractive Index
RF	Radio Frequency
SP	Surface Plasmon
SPP	Surface Plasmon Polariton
TM	Transverse Magnetic

Table of Contents

Chapter 1

Introduction

This chapter presents a general introduction to the subject of optical nanoantennas, where the primary focus would be on the rules governing the design of nanomonopoles and nanodipoles, and their agreement or disagreement with classical antenna design rules. The motivation for studying nanoantennas, in general, and nanodipoles, in particular, is addressed and some of the related literature is reviewed. At the end, the scope and organization of this thesis are introduced.

1.1 Plasmonic Nanoantennas

Although the concept of nanoantenna has been around since 1985 [1], it is only in the past decade that (due to the progress made in nanoscale fabrication methods) manufacturing of structures employing nanoantennas seems feasible. Since then, many applications have been found for nanoantennas in e.g. imaging and microscopy, spectroscopy, biosensing, and photovoltaics [1]. This growing range of applications has motivated various theoretical, numerical and experimental studies of nanoantennas. A variety of nanoantenna types have been considered ranging from nanoshells to monopoles, dipoles and bowties to Yagi-Uda nanoantennas. While a great number of these studies have concentrated on specific applications of nanoantennas, some have considered the physics behind these plasmonic structures and formed a fundamental understanding of their response behaviour.

Developing design rules for monopole, dipole, and bowtie nanoantennas has been of particular interest. Easy-to-use, yet precise rules may improve the efficiency of nanoantennas and improve their applications. Some concepts around nanoantennas have been built up in analogy to classical (RF) antennas. However, fundamental differences exist between classical antennas and

nanoantennas due to the properties of metals at IR and visible frequencies. Metals are no longer perfect electric conductors at optical frequencies but rather resemble a cold plasma [2]. Consequently they support surface plasmon polaritons (SPPs) at their surfaces. SPPs are inherently excited on nanoantennas.

This thesis was motivated by an idea of employing nanoantennas for biosensing. A periodic array of nanoantennas was considered for this application, as an isolated nanoantenna is too small comparing to the wavelength, and thus inefficient. To be able to determine the optimum nanoantenna design for the intended application, understanding the behaviour of nanoantennas, and developing appropriate design rules are important. To this end, the work in this thesis was started with a full parametric study of a periodic structure of gold nanomonopoles and nanodipoles in a piecewise homogeneous background, consisted of a silicon substrate in an aqueous medium. This background was chosen in anticipation of the biosensing application, where the sensing medium is aqueous. It was then decided that nanodipoles are more suited to the application of biosensors, because of their highly sensitive gap region which offers significant field enhancement, and their narrower spectral response compared to nanomonopoles or nanobowties, both of which improve photo detection. A schematic of a nanodipole under study is depicted in Fig. 1.

The plasmonic mode resonating in a nanomonopole was identified by comparing the electric field components in a yz cross-section of the nanomonopole, illuminated by a plane wave source from below, to the modal electric field components resonating in a plasmonic waveguide of the same cross-section. By characterizing the properties of this mode we were able to explain the trends in the response of the nanomonopoles and nanodipoles.

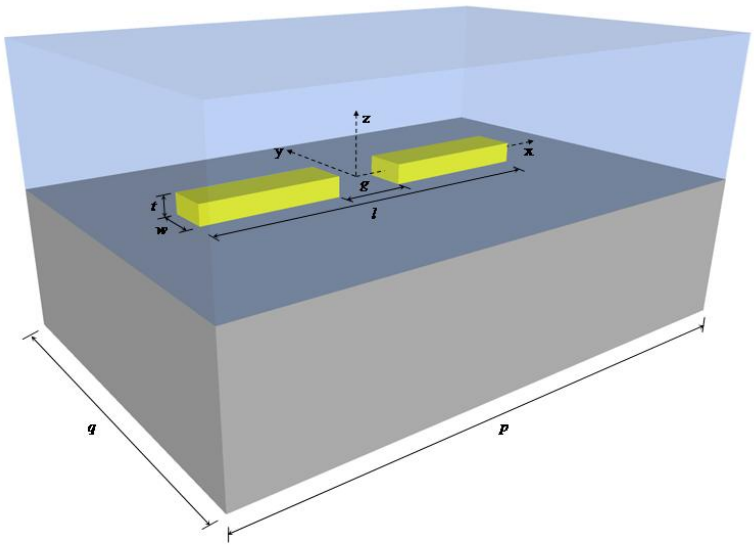

Fig.1. Schematic of a gold nanodipole on silicon, covered by water.

The effective length of a nanomonopole is evaluated from 3D FDTD results, and then an estimate of this effective length is offered by employing a length scaling factor obtained from the weighted average of the decay length of the transverse modal electric field in silicon and in water. A transmission line model is also developed to estimate the effective length of a nanodipole by considering the gap as a parallel plate capacitor. Using this model one can design dipoles of desired dimensions and material that are resonant at a required wavelength.

1.2 Literature Review

This section intends to review some of the previous theoretical and experimental work on properties of nanoantennas, on new nanoantenna designs, and on developing practical rules to simplify their design.

Different studies have attempted to achieve these goals by first understanding the properties of nanoantennas and developing theoretical models or equivalent circuits that closely reflect these properties. Among studies that focused on nanoparticles and their properties [3-5] Rechberger *et al* investigated the interactions between two gold nanoparticles [3]. Experimental results are reported for arrays of spherical nanoparticles with different inter-particle distance under perpendicular and parallel illumination. The study finds that under parallel illumination reducing the center to center distance of every pair of nanoparticles, such that the array eventually looks like an array of nanodipoles, causes a red-shift in the surface plasmon extinction peak (Fi.2), where extinction is defined as $\log_{10} T$. However, for perpendicular incidence, where the incident field is perpendicular to the long axis of the nanoparticle pairs, a small blue-shift is observed in the extinction peak as inter-particle distances are reduced. These observations are, first, qualitatively explained using a simple dipole-dipole interaction model based on the repulsive and attractive forces between the electric field of the incident light and the plasma electrons in the nanoparticles. Then a 2D quantitative study is performed based on a dipole-pair model, where the interactions of particles in the normal direction are sufficiently small to be ignored. Finally, it is shown that the experimental results are in good agreement with the results of dipole pair model calculations.

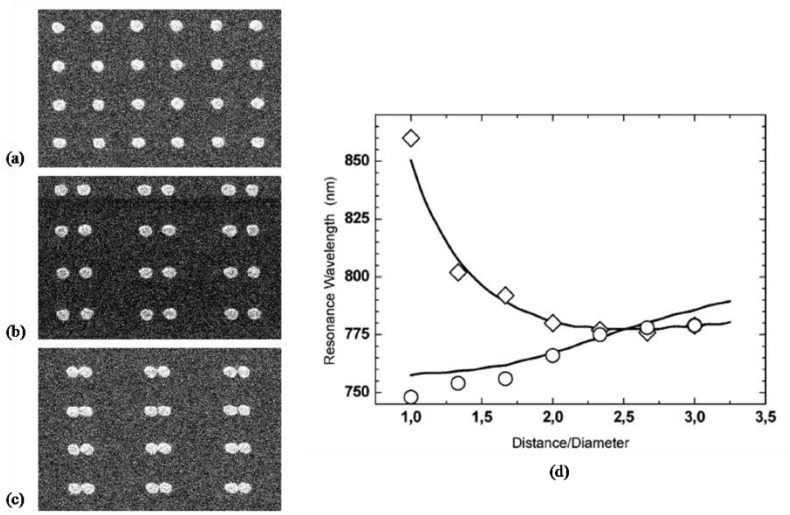

Fig.2. SEM images of particle pair samples with varying inter-particle distance (center-to-center) of (a) 450 nm, (b) 300 nm and (c) 150 nm. The particle diameter is 150 nm, the particle height is 17 nm. (d) shows spectral position of the extinction maximum vs. inter-particle distance for the full set of seven samples for the polarization directions parallel (circles) and normal (rhombs) to the long particle pair axis. Full lines show the corresponding results of the dipole-pair model calculations. (Reprinted with permission from [3] © 2003 Elsevier Science B.V.)

Nanomonopoles have attracted a lot of attention [6-10].Cylindrical rounded-end Au nanomonopoles of different length and radii are investigated by Bryant *et al.*in terms of their optical far field, near field, and scattering cross section responses [6]. By mapping the plasmon dipole resonances in Au nanomonopoles, it is demonstrated that nanomonopoles do not obey rules of the quasistatic regime, unless they are almost spherical in shape. In other words, the spectral response of a non-spherical nanoantenna is not solely dependent on the aspect ratio of the antenna, as is suggested in the quasistatic limit. Rather, the antenna response is highly sensitive to any change in the length and radius of the nanomonopoles, even if the aspect ratio remains constant. Numerical results demonstrated in this study suggest a linear increase in the resonant wavelength of the nanomonopoles as the antenna length is increased, while the radius remains fixed. Looking at the rate of shift in the resonant wavelength of antennas of different radii, one observes more significant red-shift for larger radii. On the other hand, for a fixed antenna

length and increasing radius, the resonance first blue shifts in agreement with the quasistatic predictions, and then red shifts as the radius becomes larger. The value of the radius at which this shift happens is different for different antenna lengths. One must note that the resonance of larger radii monopoles obtained from the near-field results is substantially red-shifted with respect to the resonance of the far-field results. This red-shift is due to "retardation from the resonance in far-field scattering"[6]. Numerical results are then compared to the results obtained from a simple dispersion relation for the cylindrically symmetric mode of an infinite cylinder. Results are somehow different since the dispersion relations do not consider the end effects of the nanomonopoles, which are crucial for evaluating the correct resonant length of the nanomonopoles.

Bowtie nanoantennas are investigated theoretically and experimentally [11-15]. Ding *et al.* measure intensity extinction of nanobowties [11], defined as $\log_{10} T/T_0$, where T *(*T_0*)* is the intensity of zero-order transmitted light in the present (absence) of the nanoantennas, and the normalized field distributions. Several extinction peaks are identified and associated to fundamental and higher-order resonances according to their field distributions. It is observed and explained through local mode theory and propagation of isolated SPPs along the prism edges, that increasing the bowtie angle causes the fundamental peak to blue-shift and then red-shift. These analyses are also confirmed by considering the magnitude and phase distributions of the normalized electric field parallel to the long axis of the nanobowties. Electron beam lithography is used to build periodic arrays of silver bowtie nanoantennas. The experimental results confirm the shifts of the fundamental resonance observed in simulations, although the blue-shift is not significant in experimental results. The first higher-order resonance is evident from the measurements, however, the second higher-order resonance falls outside the acquisition range of this experiment.

Fischer and Martin have comparatively studied dipole and bowtie nanoantennas [16]. In this study the spectral response of dipole and bowtie nanoantennas was investigated by varying their length, gap width, substrate index n_s, the index of their surrounding environment n_{env}, and the bowtie angle in the case of the nanobowties. While dipole antennas support only one mode, multiple modes are excited in a bowtie nanoantenna. Although changing the bowtie angle shifts the spectral position of the resonances, it does not change the field enhancement in a special trend. The field intensity is shown to be stronger in the gap of a dipole than a bowtie. The dimensions of the antenna significantly affect the spectral position of the resonance. Increasing the length of the nanoantenna redshifts the resonance, and increases the relative field enhancement in the gap for the case of dipoles. However, for bowties, where multiple resonances are present in their spectrum, each resonance must be considered individually in order to observe a clear trend. Doing so, one finds an almost linear redshift of the resonance position as a result of increasing the length of bowtie. The relative field enhancement in the gap is smaller than in the dipole, still increases by increasing the length. The authors suggest that this increase in the field enhancement is a result of stronger coupling between the two antenna arms. As the antenna is elongated, its resonance wavelength becomes larger, and hence the effective length of the gap becomes shorter, which leads to stronger coupling between two arms. Another dimension of the antenna that is examined in this study is the gap width. Decreasing the gap width of the dipole antenna shifts its resonance to longer wavelengths, while the position of the bowtie main resonance remains almost unchanged. The field enhancement is also increased by shortening the gap in both antennas. This increase is stronger in the case of dipoles. The authors suggest that “the spectrum of the bowtie antenna appears to be more determined by the resonance of the two triangular arms, rather than by the

coupling between them" [16]. As for n_s and n_{env}, increasing the indices linearly results in linear increase of the wavelength.

A theoretical wavelength scaling rule for nanomonopoles is introduced by Novotny [18]. It assumes that the nanomonopole is made of linear cylindrical segments of radius $R \ll \lambda$ and that the metal properties are described by the Drude model. A nanorod of known geometry and dielectric constant, located in a dielectric medium is considered for this study. Taking into account the charge density wave propagating along the rod and the reactance of the rod ends which increases the antenna length, the effective wavelength is calculated as

$$\lambda_{eff} = \lambda \left[\frac{k_0}{\gamma}\right] - 4R \quad (1)$$

where λ is the incident wavelength, k_0 is the free-space wave number, and γ is the propagation constant of the charge density wave, which is determined by solving for the TM_0 modes of a cylindrical waveguide. Effective wavelengths corresponding to various incident wavelengths are calculated for nanomonopoles of different radii made of Ag, Au, and Al. The effective wavelength obtained numerically by using the proposed model is then compared to the results of experiments from other studies, and a good agreement between the results is evident.

This study importantly states that the effective wavelength of nanoantennas is shorter than the free space wavelength. However, it does not give a general rule for designing antennas to be resonant at a particular free space wavelength, as would be required in practical antenna design work.

Ding *et al.* proposed an analytical model of nanoantennas based on a microcavity model [19]. Using this model, expressions are offered for the normal and longitudinal components of the electric field of the SPP mode propagating in the antenna, as well as its propagation constant, and charge and current densities. A silver hybrid dimmer nanoantenna design is presented

(Fig.3), which consists of a bowtie-like gap and two rod-like shafts. This nanoantenna is compared to a nanobowtie and a nanodipole of the same dimensions with regards to its near and far-field properties. 2D simulations are also done for all of the above mentioned nanoantennas using the boundary element method (BEM). Based on their numerical results the hybrid dimmer antenna offers higher near and far-field enhancements and Q factor than bowtie and dipole nanoantennas. In fact the hybrid dimmer nanoantenna possesses benefits originating from the long shafts of the nanodipole, which introduce strong far-field enhancements, as well as the sharp tips of the nanobowtie, which significantly improves the near-field enhancement because of high charge accumulation around the tips. 3D simulations are also done for dipole and hybrid dimmer nanoantennas using the finite-difference time-domain method. The trends of 3D simulation results agree well with those of 2D simulations. It is also noticed that by modifying the gap size of a dimmer nanoantenna one can tune its resonant wavelength. The results suggest that decreasing the size of the gap red shifts the resonance.

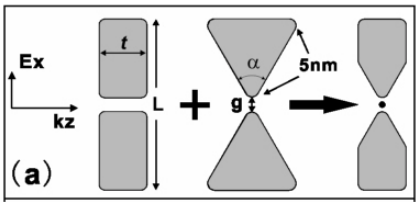

Fig.3. From right to left: schematics of the rod dimer antenna, the bowtie antenna, and the hybrid dimer antenna. (Reprinted with permission from [19] © 2009 OSA.)

Cubukcu and Capasso modeled nanomonopoles as 1D Fabry-Perot resonators for surface plasmons [20]. Through numerical analysis, it is shown that the resonance of nanomonopoles occur at integer multiples of half the effective wavelength of the SPP mode excited in the nanomonopole, rather than at half of the free space wavelength. Modal analysis of an infinitely long

nanowire of the same cross section as the nanomonopole yields the effective mode index of the nanoantenna. Then the resonance condition is described by

$$m\frac{\lambda}{2n_{eff}} = L(\lambda) + 2\delta(\lambda) \quad (2)$$

where *m* is an integer indicating the order of resonance and δ is the field penetration in vacuum "corresponding to the phase shift acquired upon reflection of the SP mode from the antenna ends. In other words, δ corresponds to the decay length of the displacement current in vacuum increasing the effective antenna length"[20]. The authors suggest that "δ is comparable to the 1/*e* decay length of the one-dimensional SP mode in the radial direction". Thus, by obtaining the n_{eff} and δ from finite element method modal calculations, one can determine the resonant antenna length using Eq.2. Results of these calculations are shown for various wavelengths and are compared with the results of finite integration method simulations, where the resonant wavelength is found for a fixed antenna length. This comparison confirms the credibility of the expression suggested in Eq.2.

Alú and Engheta studied nanoparticles as lumped nanocircuit elements, used for loading and tuning the frequency response of nanodipoles [21]. The optical impedance of these nanoloads, which may be metal or dielectric nanodisks is evaluated by

$$Z_{disk} = \frac{jt}{\omega\varepsilon\pi a^2} \quad (3)$$

where *t*, 2*a*, and ε, are respectively the height, diameter, and permittivity of the nanodisk, and ω is the frequency of the excitation electric field. In this expression ω is the frequency of the incident field parallel to the nanodisk's axis. The input impedance of the nanodipole, Z_{in}, is evaluated as the ratio between the applied voltage across the gap and the displacement current that flows through the dipole terminals. The authors suggest that Z_{in} consists of a parallel combination of the gap impedance, Z_{gap}, and Z_{dip}. Thus, by evaluating

Z_{gap} from Eq. 3 and then removing it from Z_{in} one can obtain Z_{dip}. For tuning the nanodipole at a particular frequency, one needs to design the load such that the Z_{gap} cancels the reactance X_{dip} of the dipole at the desired frequency. This can be done by changing the geometry or permittivity of the nanodisk filling the gap.

Nanodipole and nanocross plasmonic antennas were studied by Hecht *et al.* [22]. For nanodipoles of different lengths, the amplitude and phase of the electric field component localized in the gap of a dipole antenna at the wavelength of illumination is calculated with respect to the driving field in the absence of the antenna. It is shown that the enhanced filed peaks for a dipole of certain length, which is the resonant length of the nanodipoles for the incident wavelength. The phase of the field component in the gap shifts from 0° to 180°. Therefore it is possible to choose the appropriate length of a dipole to achieve desired amplitude and phase values. An asymmetric cross antenna is then proposed to convert linearly polarized propagating waves to circularly polarized fields that are confined in the common feed gap area of the antenna. By properly choosing the length of the antenna arms, one can shape the polarization of the field component inside the gap as desired.

Combining known antenna designs to produce higher field enhancement and more sensitivity Verellen *et al.* introduced the nano-cross (XI) geometry shown in Fig.4 for high sensitivity refractive index [23]. In this geometry the dipole modes in the bar (DI) and cross (Dx) and the higher order quadrupole mode in the cross (Qx) couple and produce a higher energy super-radiant anti-bonding dipole-dipole mode (ADD) with a broad line width. A lower energy sub-radiant bonding dipole-dipole mode (BDD) with a narrower line width is also produced in the XI geometry. Furthermore, coupling of DI and Qx modes results in a third hybridized mode, which is a narrow bonding quadrupole-dipole mode (BQD). Spectral overlap of the ADD and BQD modes gives rise to a destructive Fano interference, which reduces the radiation losses and

produces a narrow anti-resonant dip around the Qx resonance. Next, a Fano interference fitting model is introduced for the far field extinction spectra $E(\omega) = 1- T(\omega)$ of the nano-cross. In a series of bulk localized surface plasmon resonance (LSPR) refractive index (RI) sensing measurements sensitivities of different plasmon modes are obtained. A figure of merit (FoM) $(\delta\lambda/\delta n)/$ fwhm is then determined. For this geometry FoM values 4.6 (BDD) and 4.1 (BQD) are obtained using the line widths found by a full Fano model fit. These FoM's are the highest reported to date (according to this article) for arrays of particles (higher values are reported for single particle measurements). The strong spectral shift is attributed to the long resonant wavelengths, which are just below the water absorption band at 1900 nm, and the reduced substrate effect, due to partial removal of the substrate. Simulations show 30% increase in peak shift sensitivity for the BDD and 45% for BQD Fano modes upon etching.

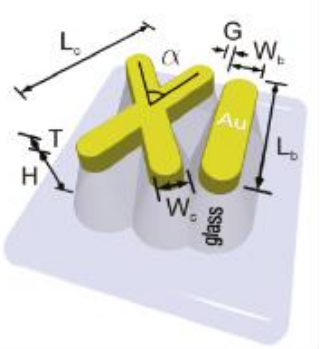

Fig. 4.Schematic of the nano-cross antenna. (Reprinted with permission from [23] © 2009 American Chemical Society.)

Tang *et al.* proposed an open-sleeve dipole nanoantenna as a photodetector at near-infrared frequencies [24]. In this device the nanodipole concentrates the incident field inside the germanium-filled gap region. The germanium nanowire is extended in the direction perpendicular to the dipole, where it is covered by two line electrodes (sleeves) to deplete the electrons and holes

created in the germanium. The high dielectric constant of the germanium in the gap significantly enhances the field inside the gap, which in turn results in enhanced photocurrent. Results of numerical simulations are confirmed by experimental results. This device provides a low-capacitance efficient sub-wavelength photodetector.

1.3 Thesis objectives and outline

This thesis intends to investigate the response of a periodic array of linear nanoantennas, namely nanomonopoles and nanodipoles, in a piecewise homogeneous medium to variations of antenna dimensions, such as length, gap size, width, thickness, and the pitch. The response of the system is defined as far-field transmittance, reflectance and absorptance. This thesis also aims at finding expressions that approximately determine the resonant length of nanomonopoles and nanodipoles.

The bulk of this thesis, chapter 2, consists of a scientific article which is submitted for publication.

Chapter 2 reports a parametric study of the response of periodic arrays of nanomonopoles and nanodipoles. An in-depth analysis of the physics of SPPs in nanomonopoles and nanodipoles is also provided by considering these nanoantennas as plasmonic metal stripe waveguides. Theoretical and equivalent circuit models are developed to predict the resonant length of nanomonopoles and nanodipoles, respectively. Chapter 3 presents conclusions, lists the thesis contributions and makes suggestions for future work.

Chapter 2

Periodic Plasmonic Nanoantennas in a Piecewise Homogeneous Background

2.1 Summary

A parametric study of periodic nanomonopoles and nanodipoles in an inhomogeneous background consisting of a silicon substrate and an aqueous medium on top is presented. By viewing the nanoantennas as plasmonic waveguides and performing modal analysis the response characteristics of the system were determined and theoretical models for predicting the resonant length of nanomonopoles and nanodipoles were offered. These models rely on the result of modal analysis.

2.2 Author Contribution

The results provided in section are to be submitted to the journal *Optics Express*. Iperformed the simulations, generated and interpreted the results, formulated the theoretical model, and wrote the manuscript.

Prof. Berini and Prof. McNamara contributed to the theoretical formulation, the interpretation of the results, and revised the manuscript.

2.3 Article

The manuscript submitted follows.

Periodic plasmonic nanoantennas in a piecewise homogeneous background

Saba Siadat Mousavi,[1] Pierre Berini,[1,2] and Derek McNamara[1]

[1]School of Electrical Engineering and Computer Science, and [2]Department of Physics, University of Ottawa, Ottawa, Ontario, Canada.

Abstract: Periodic rectangular gold nanomonopoles and nanodipoles in a piecewise inhomogeneous background, consisting of a silicon substrate and a dielectric (aqueous) cover, have been investigated extensively via 3D finite-difference time-domain simulations. The transmittance, reflectance and absorptance response of the nanoantennas were studied as a function of their geometry (length, width, thickness, gap) and found to vary very strongly. The nanoantennas were found to resonate in a single surface plasmon mode supported by the corresponding rectangular cross-section nanowire waveguide, identified as the sa_b^0 mode [Phys. Rev. B 63, 125417 (2001)]. We determine the propagation characteristics of this mode as a function of nanowire cross-section and wavelength, and we relate the modal results to the performance of the nanoantennas. An approximate expression resting on modal results is proposed for the resonant length of nanomonopoles, and a simple equivalent circuit, also resting on modal results, but involving transmission lines and a capacitor (modelling the gap) is proposed to determine the resonant wavelength of nanodipoles. The expression and the circuit yield results that are in good agreement with the full computations, and thus will prove useful in the design of nanoantennas.

OCIS codes: (240.6680) Surface plasmons; (290.5850) Scattering particles; (310.6628) Subwavelength structures, nanostructures

---

References and links

1. P. Bharadwaj, B. Deutsch, L. Novotny, "Optical antennas," Advances in Optics and Photonics **1,** 438-483 (2009).
2. L. Novotny, "Effective wavelength scaling for optical antennas," Phys. Rev. Lett. **98**, 266802 (2007).
3. W. Rechberger, A. Hohenau, A. Leitner, J. R. Krenn, B. Lamprecht, F.R. Aussenegg, "Optical properties of two interacting gold nanoparticles," Opt. Comm. **220**, 137-141 (2003).
4. E. Cubukcu and F. Capasso, "Optical nanorods antennas as dispersive one-dimensional Fabry-Perot resonators for surface plasmons," Appl. Phys. Lett. **95**, 201101 (2009).
5. H. Fischer and O. J. F. Martin, "Engineering the optical response of plasmonic nanoantennas," Opt. Express **16**, 9144-9154 (2008).
6. P. Biagioni, M. Savoini, J. Huang, L. Duó, M. Finazzi, B. Hecht, "Near-field polarization shaping by a near-resonant plasmonic cross antenna," Phys. Rev. B **80**, 153409 (2009).
7. A. Alú and N. Engheta, "Tuning the scattering response of optical nanoantennas with nanocircuit loads," Nature Photonics **2**, 307-310 (2008).
8. L. Tang, S. E. Kocabas, S. Latif, A. K. Okyay, D. S. L. Gagnon, K. C. Saraswat, D. A. B. Miller, "Nanometer-scale germanium photodetector enhanced by a near-infrared dipole antenna," Nature Photonics **2**, 226-229 (2008).
9. W. Ding, R. Bachelot, S. Kostcheev, P. Royer, R. Espiau de Lamaestre, "Surface plasmon resonances in silver Bowtie nanoantennas with varied bow angles," J. Appl. Phys. **108**, 124314 (2010).
10. A. Alú and N. Engheta, "Input impedance loading, and radiation tuning of optical nanoantennas," Phys. Rev. Lett. **101,** 043901 (2008).
11. W. Ding, R. Bachelot, R. Espiau de Lamaestre, D. Macias, A.-L. Baudrion, P. Royer, "Understanding near/far-field engineering of optical dimer antennas through geometry modification," Opt. Express **17**, 21228-21239 (2009).

12. A. Kinkhabwala, Z. Yu, S. Fan, Y. Avlasevich, K. Mullen, W. E. Moerner, "Large single-molecule fluorescence enhancements produced by a bowtie nanoantenna," Nature Photonics **3,** 654-657 (2009).
13. FDTD Solutions v. 7.5.6, Lumerical Solutions Inc., Vancouver, Canada.
14. E. D. Palik, *Handbook of Optical Constants of Solids* (Academic Press, New York, 1985).
15. D. J. Segelstein, *The complex refractive index of water*, M.Sc. Thesis, University of Missouri – Kansas City, 1981
16. R. C. Boonton Jr., *Computational Methods for Electromagnetics and Microwaves* (Wiley-Interscience, 1992)
17. T. Itoh, "Analysis of microstrip resonators", IEEE Trans. Microwave Theory Tech. **22**, 946-952 (1974).
18. P. Berini, "Plasmon-polariton waves guided by thin lossy metal films of finite width: bound modes of symmetric structures," Phys. Rev. B **61**, 10484-10503 (2000).
19. P. Berini, "Plasmon-polariton waves guided by thin lossy metal films of finite width: bound modes of asymmetric structures," Phys. Rev. B **63**,125417 (2001).
20. D. M. Pozar, *Microwave Engineering* (Wiley, 2005).
21. H. G. Booker, *Electromagnetism* (Peter Peregrinus Ltd, 1982)

1. Introduction

Nanoantennas have been widely investigated, both experimentally and numerically, during the past decade. Nanomonopoles, nanodipoles and nanobowties have been of particular interest. Although there are some conceptual similarities between optical nanoantennas and classical microwave antennas, the physical properties of metals at optical frequencies dictate applying a different scaling scheme. Moreover, feeding procedures are very different between classical and optical nanoantennas, since driving nanomonopole, nanodipole, and nanobowtie nanoantennas using galvanic transmission lines is not an option, due to their small size. Instead, localised oscillators or incident beams are often used to illuminate nanoantennas [1].

One of the primary differences between classical monopoles and dipoles and their optical counterparts is their resonant length which is considerably shorter than $\lambda/2$ [2], where λ is the free-space incident wavelength. In [2] Novotny introduces useful analytical expressions for wavelength scaling of free-standing cylindrical nanomonopoles of different radii surrounded by a dielectric medium. The results of this study, however, are not easily applicable to other nanoantenna geometries such as dipoles and bowties, or non-cylindrical nanoantennas. Adding a substrate, which is often required in practice, also necessitates some modifications to wavelength scaling expressions.

As in classical antennas, the spectral position of the resonance in the optical regime depends strongly on the geometry of the antennas. Antenna length has been investigated as a crucial tuning parameter in nanomonopoles, nanodipoles, and nanobowties [3-6]. Capasso and Cubukcu proposed a resonant length scaling model for free-standing cylindrical nanomonopoles by using the decay length of the surface plasmon mode excited in the corresponding plasmonic waveguide as the scaling factor [4]. In the case of dipoles and bowties the gap size and gap loading play an important role in determining the position of resonance [3, 5-11]. Alu and Engheta have looked at nanoantennas as lumped nanocircuit elements and investigated some of their properties such as optical input impedance, optical radiation resistance, and impedance matching [7, 10]. In these studies the gap is considered as a lumped capacitor, which is connected in parallel to the nanodipole. This model identifies the gap length and gap loading as additional tuning parameters of nanodipoles. Fischer and Martin show that in nanodipoles, decreasing the gap shifts the resonance towards the red region of the spectrum, whereas in the case of bowties the resonance hardly shifts as a result of changing the gap [5]. High intensity fields in the dipole and bowtie gaps are strongly sensitive to the index of the material inside the gap [5, 7]. Also the effects of variations in the bow angle of a bowtie antenna on its spectral response have been investigated numerically and experimentally [5, 9], showing that the bow angle can be used as a tuning parameter.

Semi-analytical investigations have been done on nanodipole, nanobowtie, and hybrid dimer nanoantennas based on a microcavity model [11], and analytical expressions were suggested for surface and charge densities corresponding to the SPP mode propagating in the nanoantenna, which in turn represent near- and far-field properties of these nanoantennas.

Nanoantennas, in general, and the three above-mentioned types in particular, have found many applications in nanoscale imaging and spectroscopy [1], photovoltaics [1], and biosensing [12]. With a growing range of applications, developing precise, yet practical design rules for nanoantennas seems essential.

Although many theoretical and experimental studies have been carried out on various aspects of nanoantennas and their applications, a systematic study of their spectral response to variations in design parameters is lacking in the literature. In this paper, we present a full parametric study of the spectral response of infinite arrays of rectangular gold nanomonopoles and nanodipoles on a silicon substrate covered by water. (The materials were selected in anticipation of an eventual biosensing application to be described elsewhere; however, the study remains otherwise generic.) We vary the nanoantenna length (l), width (w), thickness (t), and, in the nanodipole case, the gap length (g), as well as the vertical and horizontal distance (p, q) between any two adjacent nanoantennas in an infinite array. Physical insight into the resonant response of arrays of nanoantennas is then provided through modal analysis of the corresponding plasmonic nanowire waveguides. A simple rule is proposed to determine the effective length of a nanomonopole in a piecewise homogeneous background from the modal properties of the corresponding nanowire. An equivalent circuit using transmission lines and a capacitor is proposed for the nanodipoles, with the capacitor taking into account the effects of the gap. This simple rule and model should become helpful aids in the design of such nanoantennas. (In the remainder of this paper we refer to nanoantenna, nanomonopole and nanodipole simply as antenna, monopole and dipole.)

The antenna geometry and the method used in its study are discussed in Section 2. The parametric study of monopole and dipole arrays is presented in Section 3. Section 4 discusses the operation of the antennas from a modal viewpoint and gives expressions for the resonant length of monopoles and the equivalent circuit of dipoles. Section 5 gives our conclusions.

2. Geometry and Methods

Figure 1 gives a sketch of the dipole geometry under study. The array cell is symmetric about the x and y axes. An infinite array is constructed by repeating the cell along x and y with pitch dimensions p and q (respectively). A plane wave source having an electric field magnitude of 1 V/m, located in the silicon substrate, illuminates the array from below at normal incidence.

The finite difference time domain (FDTD) method [13], with a 0.5×0.5×0.5 nm^3 mesh in the region around the antenna, was used for all simulations. Palik's material data [14] were used for gold and silicon, and Segelstein's data [15] for water. Transmittance and reflectance reference planes were located 2.5 μm above and below the silicon-water interface, respectively, parallel to the interface. (A convergence analysis was performed where the resonant wavelength of an array was tracked as a function of mesh dimensions in the neighborhood of the antenna. Mesh dimensions were halved successively, starting from a 2×2×2 nm^3 cubic mesh to a 0.25×0.25×0.25 nm^3 cubic mesh, over which the resonant wavelength was observed to trend monotonically. The wavelength of resonance for mesh dimensions of zero (infinitely dense) could thus be extrapolated using Richardson's extrapolation formula [16]. Comparing this extrapolated wavelength to the wavelength obtained for a finite mesh of 0.5×0.5×0.5 nm^3 reveals a ~2% error, which considering the broad spectral response of the structures of interest, was deemed acceptable.)

The transmittance T was calculated as a function of frequency (wavelength) using:

$$T(f) = \int_S \mathrm{Re}\{\boldsymbol{P^m}(f)\} \cdot \boldsymbol{ds} \Big/ \int_S \mathrm{Re}\{\boldsymbol{P^s}(f)\} \cdot \boldsymbol{ds} \qquad (1)$$

where $\boldsymbol{P^{m,s}}$ is the Poynting vector at the monitor and source locations, f is the frequency and S is the surface of the reference plane where the transmittance is computed [13]. Eq. (1) was

also used to compute the reflectance R of the system by changing S to the appropriate reference plane. The absorptance is then determined as A=1-T-R.

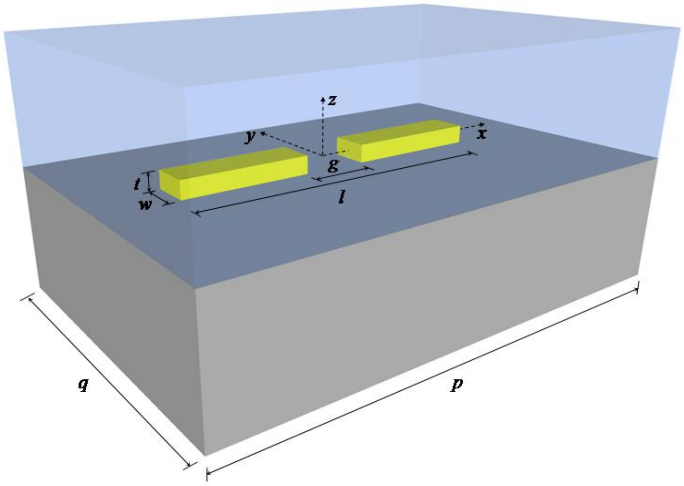

Fig. 1. Geometry of a unit cell of the system under study: a Au rectangular dipole antenna on a silicon substrate covered by water. A plane wave source illuminates the antenna in the z-direction from within the substrate.

Throughout this paper the resonant wavelength (λ_{res}) refers to the free-space wavelength at which the transmittance curve reaches its minimum value. Reflectance resonance and absorptance resonance refer to the wavelengths at which reflectance and absorptance reach their minima, respectively (in general these three resonant wavelengths are different).

3. Parametric Study of an Array of Antennas

A rigorous analysis of the design parameters of the two types of antennas is carried out by varying one design parameter at a time and monitoring the response of the system. Results are presented for monopole and dipole antennas in Sec. 3.1 and Sec. 3.2, respectively. These results will be useful as a guideline for design and to relate the antenna performance to its geometry. The minimum values of g, t and w reflect approximate limitations of an eventual fabrication process.

3.1 Periodic Array of Monopoles

An array of monopoles (g = 0) with fixed pitch is a relatively simple, yet, effective resonant structure. Here, we investigate such an array by determining the influence of changing each design parameter (independently) on the system response, while keeping the other parameters fixed, including the pitch (p×q)which is maintained to 300×300 nm^2. We consider variations of length l, width w and thickness t of the monopoles.

3.1.1 Length (l)

Length is one of the main design parameters of antennas. As shown in Fig. 2, increasing the length of a monopole shifts its transmittance, reflectance, and absorptance resonances to longer wavelengths. The red shift is expected by analogy to classical antennas, where resonance occurs when the antenna length is roughly half a wavelength. Increasing the length thus increases the wavelength at which the antenna is resonant. Increasing the length also decreases slightly the absorptance in the monopoles and broadens the absorptance response.

Field enhancements (not shown here) very much depend on the location along the monopoles; the only regions with field enhancement are the ends of the monopole. In contrast, as discussed in Sec. 3.2, the gap region of dipoles generates highly enhanced fields, making dipoles very sensitive to changes in the gap region.

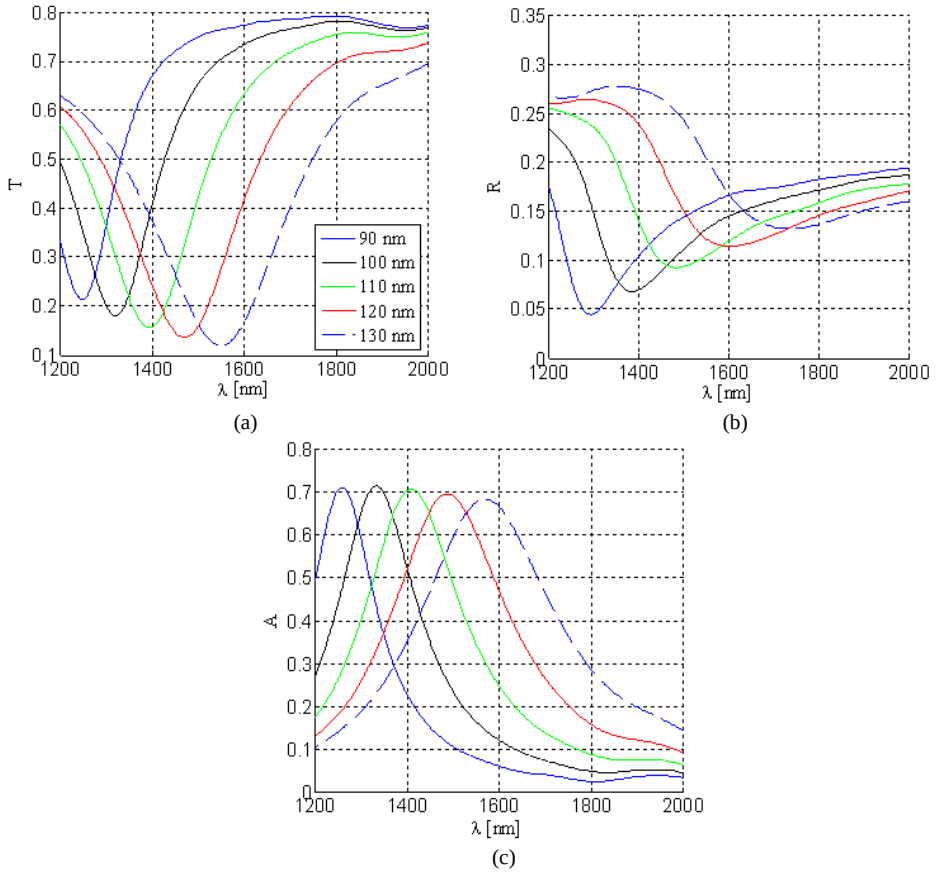

Fig. 2. (a) Transmittance, (b) reflectance and (c) absorptance vs wavelength for monopoles of w=20 nm, t=40 nm and variable l (given in legend inset to (a)).

3.1.2 Width (w)

Monopole width is another design parameter. Considering the system response to changes in width w, shown in Fig. 3, we note that increasing the latter blue-shifts the transmittance, reflectance and absorptance resonances. We also note that the amount of shift decreases as $\Delta w/w$ decreases. The reasons for this behaviour will become clear in Sec. 4, where we examine the modal characteristics of the corresponding nanowire waveguides.

The absorptance level, as shown in Fig. 3(c), does not follow a linear trend with increasing monopole width. A maximum value of absorptance is evident, unlike the linearly decreasing trend that we observed as a result of increasing the length of the monopoles.

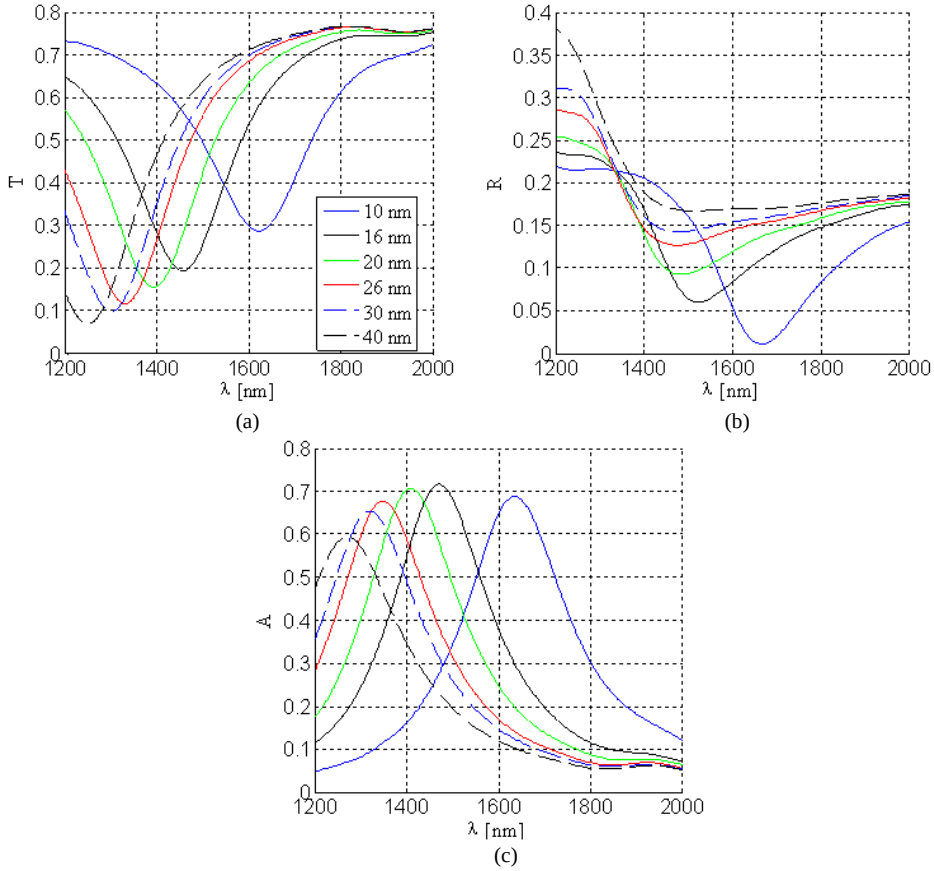

Fig. 3. (a) Transmittance, (b) reflectance and (c) absorptance vs wavelength for monopole antennas of l=110 nm, t=40 nm and variable w (given in legend inset to (a)).

3.1.3 Thickness (t)

The response of the system to variations in thickness t is shown in Fig. 4. As with the width, increasing the thickness causes a blue-shift in the resonant wavelengths. The absorptance peaks at t = 30 nm, while the amount of shift of the resonant wavelength decreases as $\Delta t/t$ decreases. This behavior will also be explained in Sec. 4 where we discuss the modal characteristics of the corresponding nanowire waveguides.

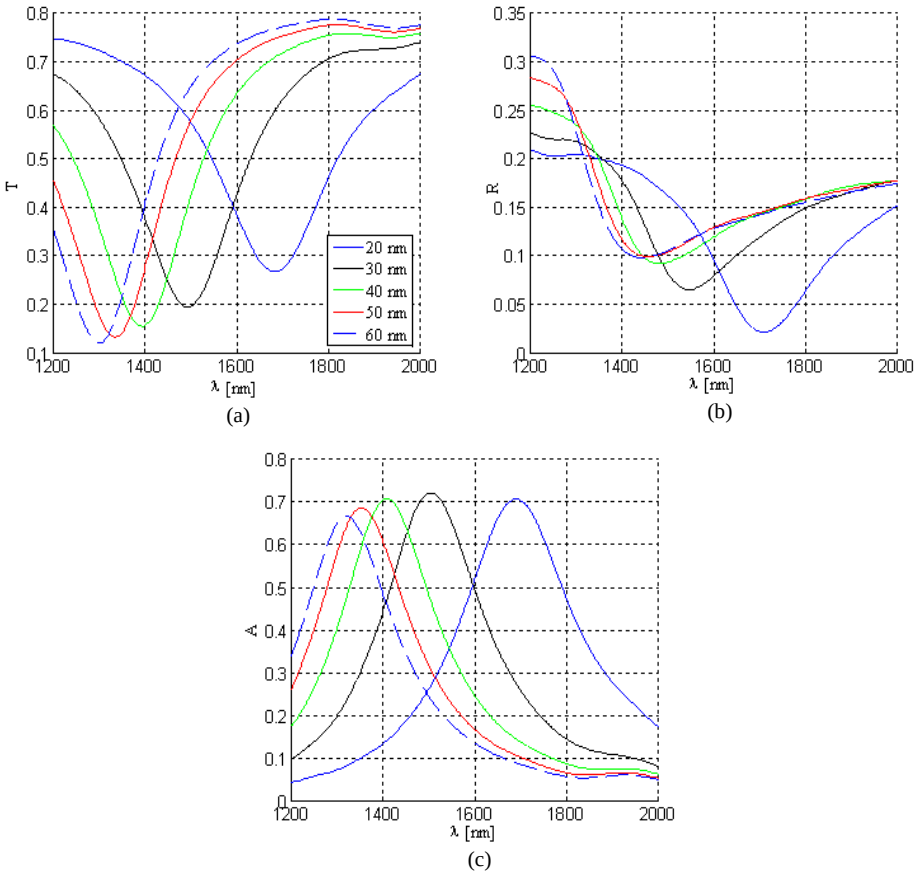

Fig. 4. (a) Transmittance, (b) reflectance, and (c) absorptance vs wavelength for monopole antennas of l=110 nm, w=20 nm and variable t (given in legend inset to (a)).

3.2 Periodic Array of Dipoles

A region of highly localised, enhanced fields is one of the main attractions of dimer antennas, such as dipoles and bowties. Here we chose to study a periodic array of dipoles not only because of its similarities to an array of monopoles, but also for its advantage over monopoles, namely, having a gap region with highly concentrated fields, and its sharper wavelength response compared to bowties and monopoles. In this section we study the response of an array of dipoles to variations in individual dipole length, gap, width and thickness.

3.2.1 Length (l)

Figure 5 shows the response of a periodic array of dipoles to changes in the length from l=190 to 280 nm in steps of 10 nm, while w, t, g, p and q remain fixed. As is evident from Fig. 5(a), increasing the length of the dipole red-shifts the resonant wavelength, decreases the amount of power transmitted at resonance, and increases the level of reflectance of the system, but the absorptance remains almost unchanged.

Elongating the dipole while keeping the pitch constant means increasing the proportion of gold surface area covering the silicon-water interface (and thus intercepting a greater fraction of the incident wave) resulting in more reflection and less transmission. The electric field enhancement on resonance is calculated at the center of the gap, 3 nm above the silicon-water

interface (a representative location in the gap in H_2O) with respect to the electric field at the same location in the absence of the antenna, and is shown in Fig. 5(d). The electric fields in the absence of the antenna are computed at the λ_{res} of each corresponding dipole. The difference between the electric fields at different wavelengths in the absence of the dipole is, however, negligible, as expected. The field enhancement, although slightly decreasing as l increases, is relatively constant over the range of lengths, which implies the electric field distribution in the gap does not change much by increasing the length of the dipoles. However, as the antenna length increases, the coupling between any two adjacent antennas (along the x-axis) increases. This means higher field localisation at antenna ends, which leads to slightly less field localisation in the gap as the antenna length increases, explaining the trend of Fig. 5(d). This is also confirmed in Fig. 6 which shows the magnitude of the x-component of the electric field along the antenna length, taken at the silicon-gold interface at $y = 0$ at the resonant wavelength for each case. This figure clearly shows coupling between two neighbouring dipoles for this pitch p. As the length increases the distance between the ends of any two adjacent dipoles becomes smaller. When the dipole is long enough, such that the distance between two neighbouring antennas is the same as the gap length, the electric fields at the gap are equal to those at the ends.

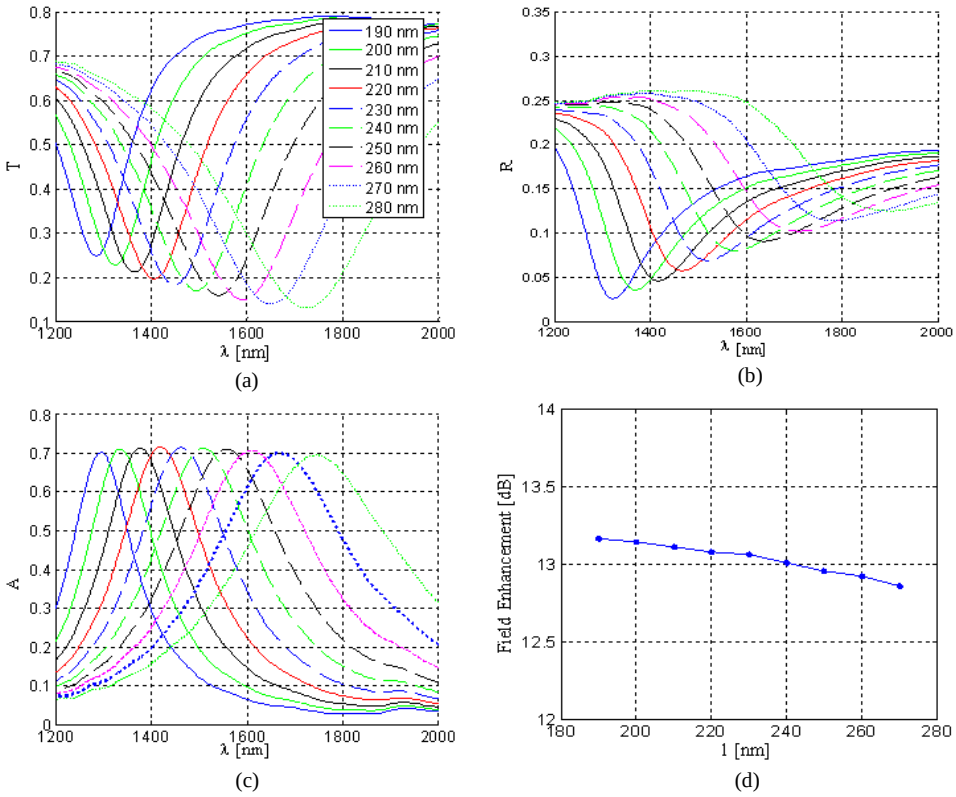

Fig. 5. (a) Transmittance, (b) reflectance and (c) absorptance vs wavelength for a dipole of g=20 nm, w=10 nm, t=40 nm, p=q=300 nm and variable l (given in legend inset to (a)). Part (d) shows $10\log(|E_x|/|E_{inc}|)$ where E_x is taken at x=0, y=0, z=3 nm on resonance and E_{inc} is the incident field at the same location and wavelength in the absence of the antenna.

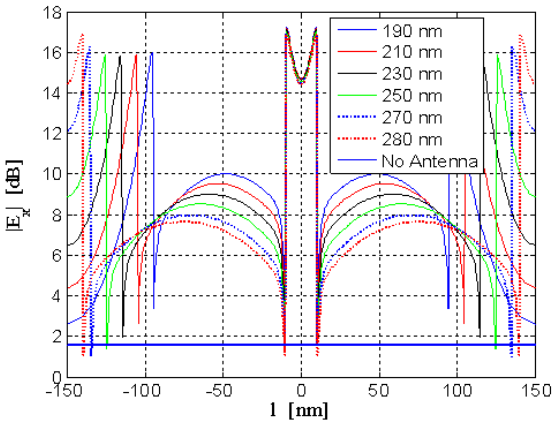

Fig. 6. $|E_x|$ along the length of the antenna for different l values (given in legend in inset); $|E_x|$ is also shown in the absence of the antenna.

Figure 7 shows the electric field distribution of dipole over the *x-y* cross-section close to the silicon-gold interface, slightly inside the gold. Fig. 7(b) shows the field distribution on resonance, while Figs. 7(a) and (b) show the fields at wavelengths below and above λ_{res}. The magnitude of the electric field is clearly enhanced on resonance.

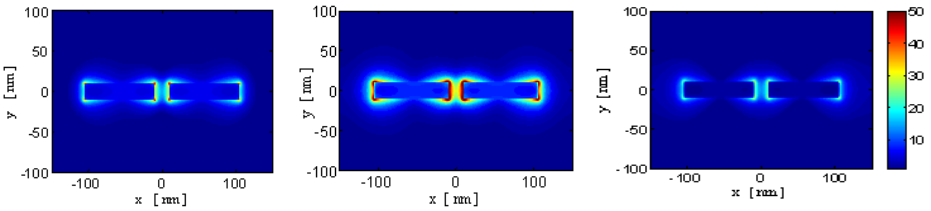

(a) (b) (c)

Fig. 7. $|\boldsymbol{E}| = \sqrt{|E_x|^2 + |E_y|^2 + |E_z|^2}$ on the *x-y* plane 3 nm inside a gold dipole of dimensions l= 210 nm, w=20 nm, t=40 nm, p = q = 300 nm, and g=20 nm at (a) λ= 1250 nm, (b) $\lambda = \lambda_{res}$=1366 nm, and (c) λ=1700 nm.

3.2.2 Gap (g)

Figures 8(a)-(c) show the transmittance, reflectance and absorptance of the system as a function of wavelength for different antenna gap lengths g. While the transmittance increases with increasing gap length, the reflectance decreases, as the proportion of gold covering the surface becomes smaller. Increasing the gap of an array of dipoles moves the response from the limit g = 0, corresponding to an array of monopoles of length l, to the limit $g = p - l$, corresponding to an array of monopoles of length $(l - g)/2$. At this limit, the length of the antennas are reduced to less than a half of their original value, which according to classical antenna theory implies a blue-shift in the resonance. This is indeed observed in the results of Fig. 8. There is also a capacitance associated with the gap that explains in part the wavelength shift, as discussed in Sec 4.4.

The field enhancements, shown in Fig. 8(d), are calculated as described in Sec. 3.2.1. A steep decrease in the field enhancement is evident as the gap increases, which is corroborated by the field distributions of Fig. 9.

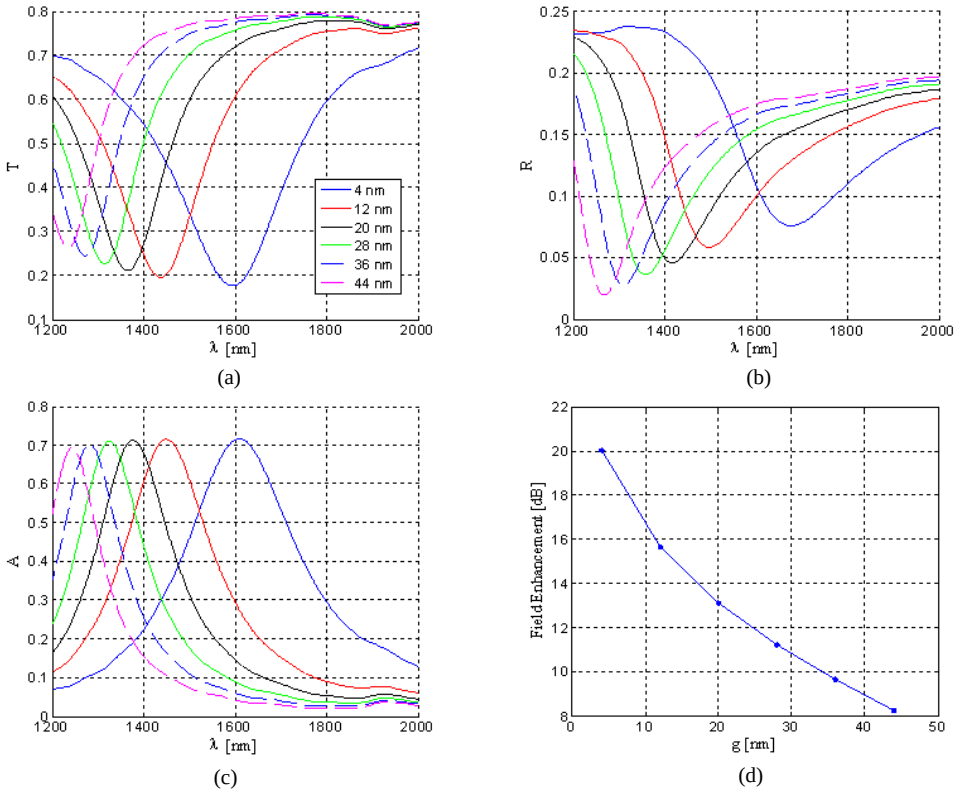

Fig. 8. (a) Transmittance, (b) reflectance and (c) absorptance vs wavelength for dipole antennas of l=210 nm, w=20 nm, t=40 nm, p=q=300 nm and variable g (given in legend inset to (a)). Part (d) plots 10log($|E_x|/|E_{inc}|$) where E_x is taken at x=0, y=0, z=3 nm on resonance and E_{inc} is the incident field at the same location and wavelength but with the antenna removed.

We note from Fig. 9 that in dipoles with a small gap, fields are appreciably larger in the gap than at the ends. However, as the gap gets larger the fields are almost equally distributed at both ends of a single arm of the dipole. Localised fields in the gap region of dipoles make small-gap antennas highly sensitive to changes in the gap region.

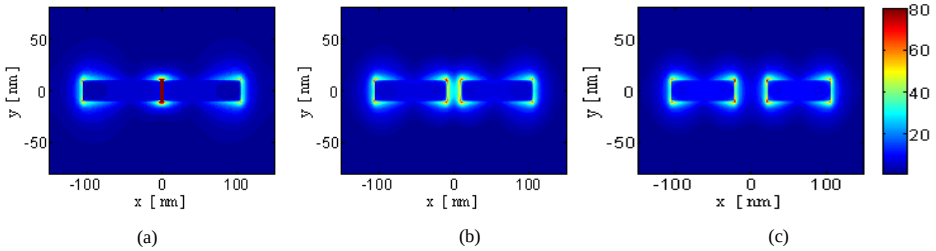

Fig. 9. $|\boldsymbol{E}| = \sqrt{|E_x|^2 + |E_y|^2 + |E_z|^2}$ on the x-y plane 3 nm inside a gold dipole having l = 210 nm , w = 20 nm , t= 40 nm and p = q = 300 nm for (a) g= 4 nm, (b) g= 20 nm and (c) g= 44nm.

3.2.3 Width (w)

Figure 10 shows the transmittance, reflectance and absorptance of the array of dipoles as a function of wavelength for different antenna widths *w*. From Fig. 10(a) one can clearly see that increasing the width of the antenna from 4 to 60 nm blue-shifts the position of the resonance and lowers the level of transmittance at resonance. Figs. 10(b) and (c) show a similar shift in the reflectance and absorptance, respectively. The amount of shift decreases as $\Delta w/w$ decreases. This property is explained in terms of the characteristics of the mode excited in the dipole arms, as will be discussed in Sec.4. Fig. 10(d) shows field enhancements calculated at the center of the dipole gap, 3 nm above the silicon-water interface. One can clearly see that w=20 nm gives the maximum enhancement of the electric field, while w=4 nm yields the minimum enhancement.

From Fig. 11, which shows the total electric field over the *x*-*y* cross-section of the antenna where the field enhancements are calculated, one can clearly see that at w=20 nm the fields at the center of the gap reach their largest value, resulting in the strongest field enhancement. However, for very small and very large widths, although fields are strongly localised at the extremities, the non-uniform distribution of fields over the gap yields smaller field values at the center of the gap.

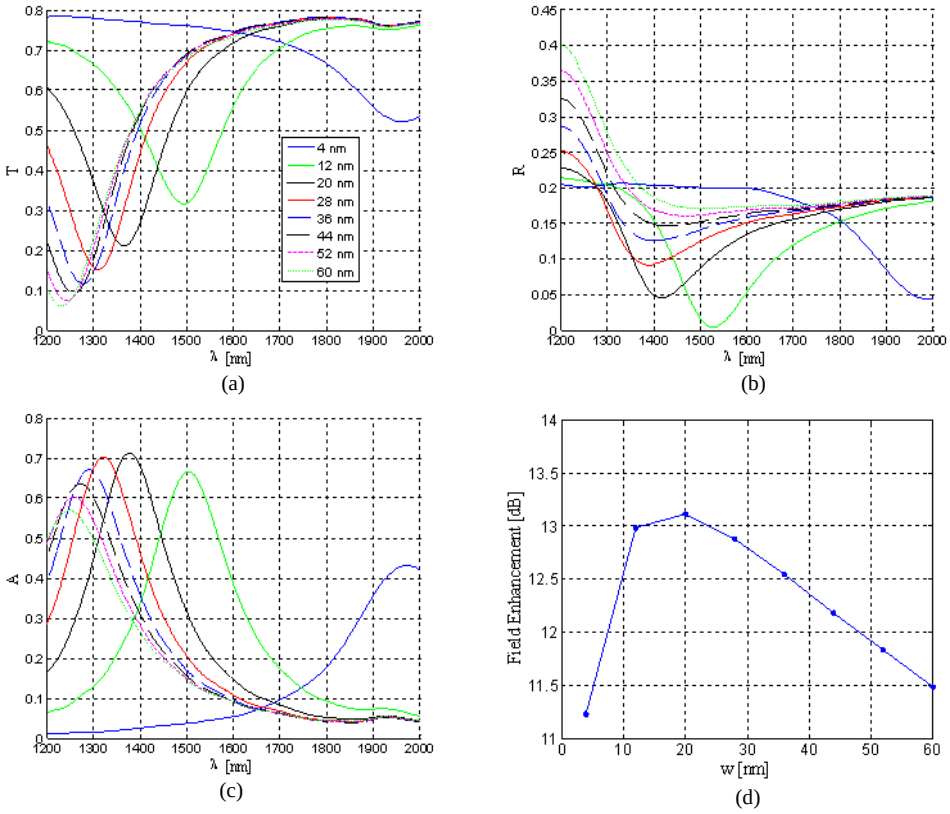

Fig.10. (a) Transmittance, (b) reflectance and (c) absorptance vs wavelength for dipole antennas of l=210 nm, t=40 nm, g=20 nm, p=q= 300 nm and variable w (given in legend inset to (a)). Part (d) plots $10\log(|E_x|/|E_{inc}|)$, where E_x is taken at x=0, y=0, z=3 nm on resonance and E_{inc} is the incident field at the same location and wavelength in the absence of the antenna.

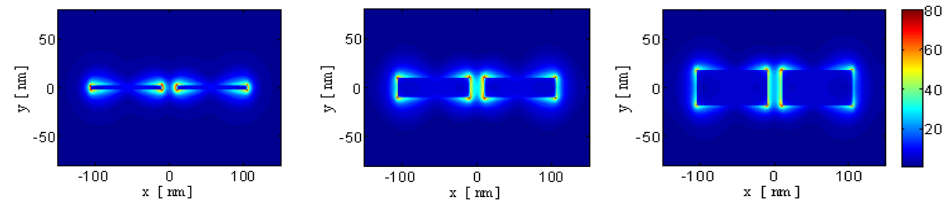

(a) (b) (c)

Fig. 11. $|\boldsymbol{E}| = \sqrt{|E_x|^2 + |E_y|^2 + |E_z|^2}$ on the *x*-*y* plane 3 nm inside a gold dipole having l = 210 nm, g = 20 nm, t= 40 nm and p = q = 300 nm for (a) w= 4 nm, (b) w= 20 nm and (c) w= 36 nm.

In Fig. 12 the total electric field is shown over a *y*-*z* cross-sectional plane taken at the middle of a dipole antenna arm. As the antenna gets wider, the field becomes less intense across the *y*-*z* plane, and less coupling occurs between the fields localised at the left and right edges. This establishes two separate localised field regions (Fig. 12(c)), as opposed to one high intensity region that exists in narrow-width dipoles (Fig. 12(a)). Clearly, the antenna fields are strongly dependant on *w*.

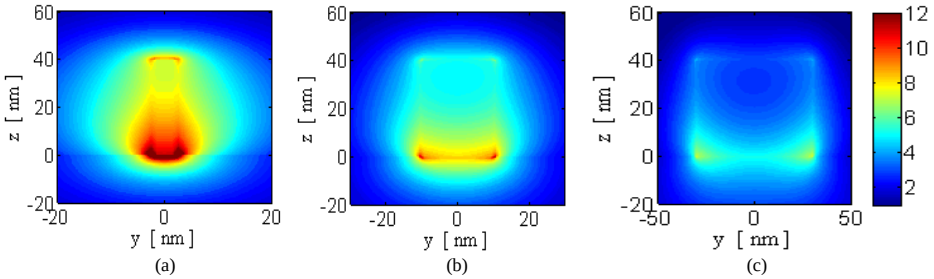

(a) (b) (c)

Fig. 12. $|\boldsymbol{E}| = \sqrt{|E_x|^2 + |E_y|^2 + |E_z|^2}$ on the y-*z* plane at the middle of a gold dipole arm having l = 210 nm, g = 20nm, t= 40 nm and p = q = 300 nm for (a) w= 4 nm, (b) w= 20 nm and (c) w= 60 nm.

3.2.4 Thickness (t)

A similar study was performed to understand the effects of changing the thickness t of the dipole. Increasing the thickness causes a blue-shift in the resonances, as shown in Fig. 13. The amount of shift decreases for decreasing $\Delta t/t$. This property is explained in terms of the characteristics of the mode excited in dipole arms, as will be discussed in Sec. 4. Fig. 13(d) shows field enhancements calculated at the center of the dipole gap, 3 nm above the silicon-water interface. One notes that the field enhancement does not depend strongly on thickness.

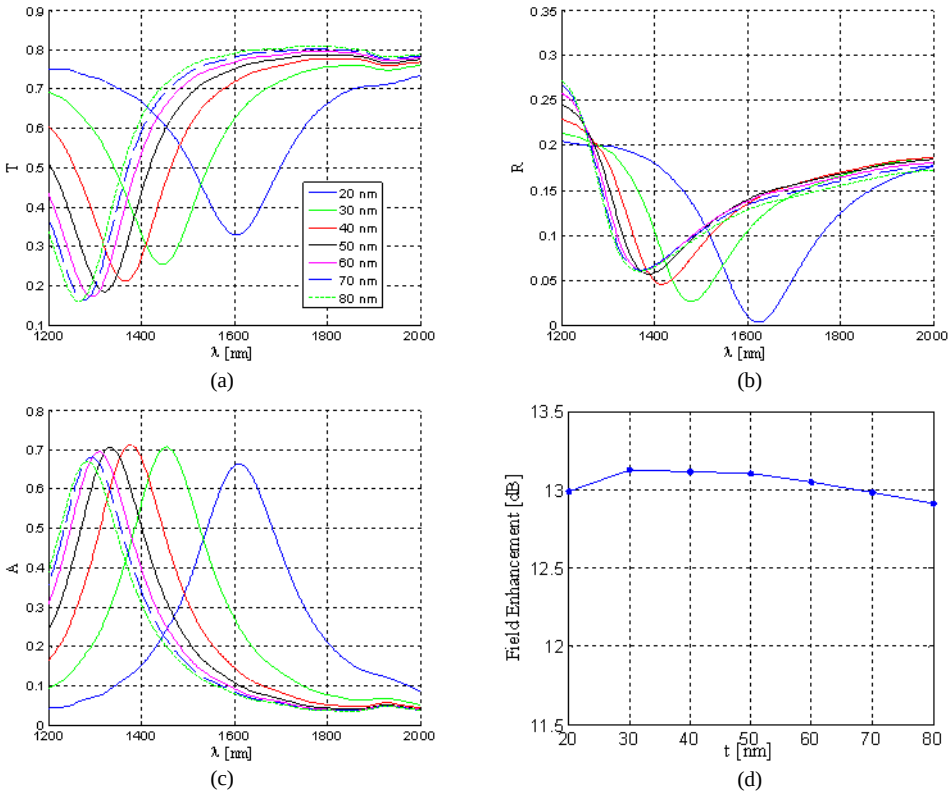

Fig. 13. (a) Transmittance, (b) reflectance, and (c) absorptance versus wavelength for dipole antennas of l=210 nm, w=20 nm, g=20 nm, p=q=300 nm and variable t (given in legend inset to (a)). Part (d) plots $10\log(|E_x|/|E_{inc}|)$, where E_x is taken at x=0, y=0, z=3 nm on resonance and E_{inc} is the incident field at the same location and wavelength in the absence of the antenna.

In Fig. 14 the total electric field is shown over a y-z cross-sectional plane taken at the middle of a dipole antenna arm. As the antenna gets thicker, the field becomes more localised near the silicon-water interface but does not change appreciably in character (compared to changes in width - Fig. 12).

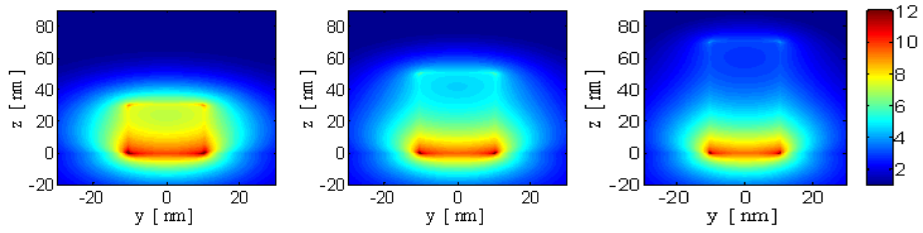

Fig. 14. $|\boldsymbol{E}| = \sqrt{|E_x|^2 + |E_y|^2 + |E_z|^2}$ on the y-z plane at the middle of a gold dipole arm having l =210 nm, g = 20 nm, w= 20 nm and p = q = 300 nm for (a) t= 30 nm, (b) t= 50 nm and (c) t= 70 nm.

3.2.5 Alignment of Transmittance, Reflectance and Absorptance Extrema

From Figs. 2-5, 8, 10 and 13, we note that the wavelength corresponding to the minimum of the transmittance curve does not lineup with extrema in the reflectance or the absorptance curves for a given array of dipoles. To determine the reason, the imaginary parts of the

permittivity of gold and water were made zero, one at the time. Results are shown in Fig. 15, where one could clearly see that the positions of the minima in the transmittance and reflectance curves are aligned if the permittivity of gold is purely real, which implies that the misalignment is due to the absorption of gold. As the imaginary part of the permittivity of gold is forced to zero, no energy is absorbed by the antennas, which makes the absorptance close to zero (small losses remain in water); thus the illuminating beam is partially transmitted and reflected. This also shows that most of the energy in the system is absorbed by the gold and not by the water. In fact, water absorption is negligible over most of the wavelength range shown (for the reference planes adopted). Fig. 15 shows the transmittance, reflectance and absorptance curves on the same scale, which clearly demonstrates their relative values.

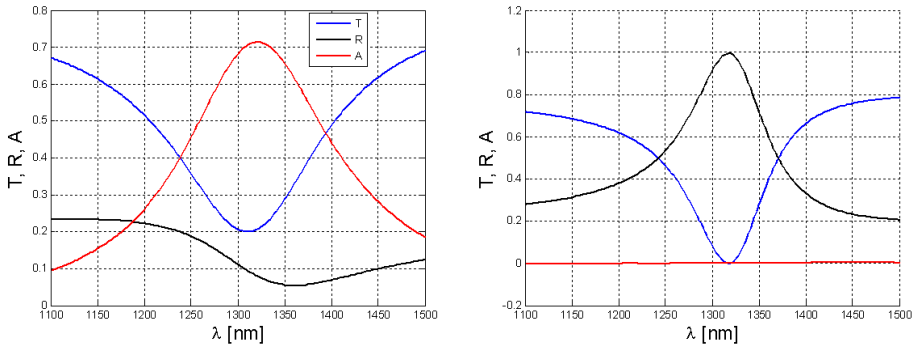

Fig. 15. Transmittance, reflectance and absorptance of an array of dipoles, using (a) the full material properties of silicon, gold and water, and (b) forcing the imaginary part of the permittivity of gold to zero.

3.2.6 Full Width at Half Maximum

In this section we consider the full-width-at-half-maximum (FWHM) of the absorptance response of the arrays. We determine the FWHM by finding the difference between the two wavelengths corresponding to the half value of the peak of each response curve. These results are shown on the left vertical axes ($\Delta\lambda$) in Figs. 16(a)-(d) as a function of each design parameter. We convert the $\Delta\lambda$ values to the frequency domain using

$$\Delta v = \frac{c}{\lambda_{res}^2}\Delta\lambda \tag{2}$$

where c is the speed of light in free-space and $v = \omega/(2\pi)$is the frequency, and we plot this on the right axis of each figure.

Fig. 16(a) shows an increasing FWHM as the length of the dipoles increases. This is caused by an increase in the loss of the antennas due to their longer length, resulting in broadening (see also Sec. 4.2). The same argument holds for the change in FWHM as a function of gap length: by increasing the length of the gap in a dipole of fixed length, we effectively make the dipole arms shorter, thus decreasing the loss and the FWHM, as shown in Fig. 16(b). The FWHM is shown in Figs. 16(c) and (d) as a function of dipole width and thickness. Here, as the length of the dipoles is fixed, the only contributing factor is the change in the attenuation of the mode resonating in the antenna - it increases as λ decreases (see Sec 4.2). Thus, by increasing the width and thickness of dipoles, their FWHM (Δv) decreases.

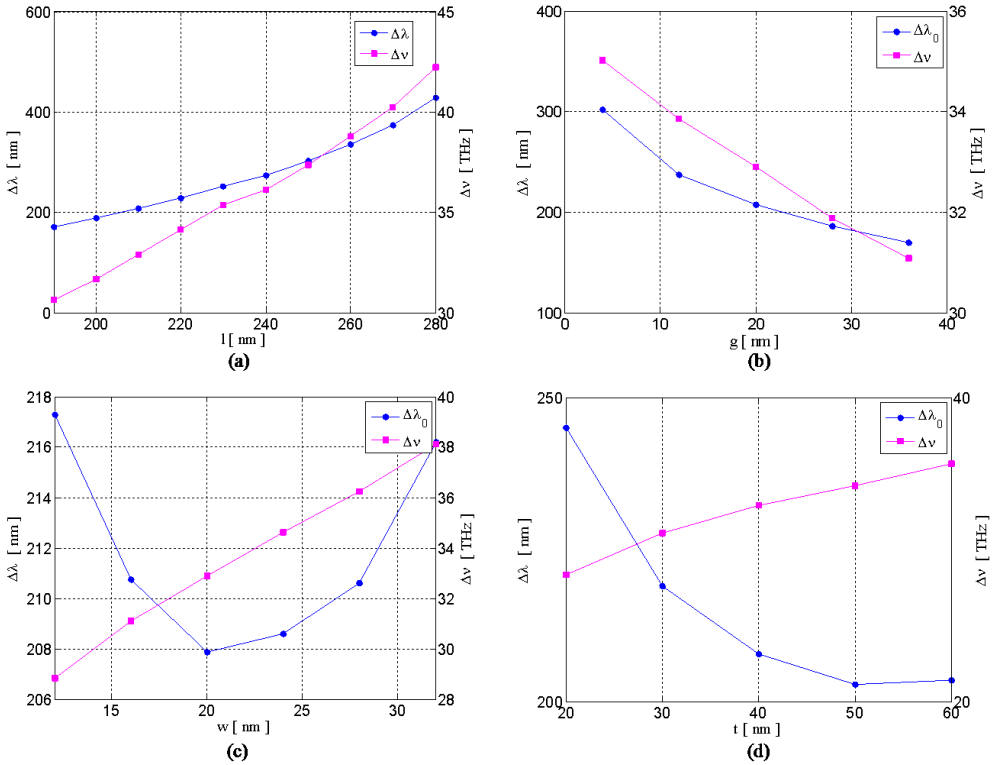

Fig. 16. FWHM of the absorptance response as a function of (a) length *l*, (b) gap *g*, (c) width *w*, and (d) thickness *t*. The left axis shows the FWHM calculated as Δλ and the right axis shows the corresponding Δυ.

3.3 Field Decay from the Monopole Ends - Effective Length L_{eff}

Generally, resonance depends on a balance of stored electric and magnetic energies. Energy is stored not only over the physical length of a monopole but also in the fields decaying at its ends (as in microstrip resonators at microwave frequencies *viz*. the end fringing fields [17]). Thus, a monopole appears to have an effective length (L_{eff}) which is greater than its physical length. The longitudinal electric field component, E_x, is used to measure the 1/*e* field decay beyond the antenna ends. Fig. 17 shows E_x along the *x*-axis at y=0 for several heights (z). The average of these decay lengths is denoted by δ_a (also termed the length correction factor) and used to determine the effective monopole length L_{eff} as:

$$L_{eff} = l + 2\delta_a \tag{3}$$

We could also take the electric displacement D_x or the polarization density P_x to measure the length correction factor. Not surprisingly, the measures yield essentially the same value regardless of their definition. The results show that the antenna fields (which can be thought of as equivalent current densities) penetrate the background a non-negligible distance (~20 nm) beyond the ends of the monopole. In Sec. 4, we propose an alternative method to estimate δ_a, which does not require FDTD modelling.

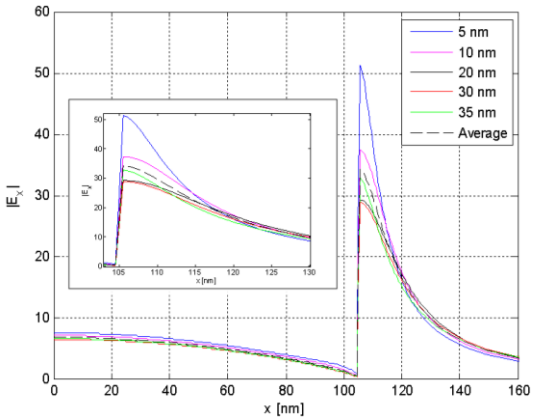

Fig. 17. Electric field E_x along the x-axis of a monopole of l=210 nm, w= 20 nm, t = 40 nm and p=q= 300 nm, at y= 0 for several heights z (indicated in the legend). The average of E_x at the z locations of this figure (and for z= 15 and 25 nm) is also shown. The inset shows E_x at the physical end of the antenna, where the field is discontinuous.

4. Surface Plasmon Mode of the Antennas

The antennas investigated in the previous section are formed from rectangular cross-section Au nanowires in a piecewise homogeneous background. It is known that a thin, wide metal stripe in a symmetric [18] or asymmetric [19] background supports several surface plasmon modes. The nanowire comprising the antennas is very similar in structure to the asymmetric stripe [19]. It is thus surmised that it operates (and resonates) in a surface plasmon mode of the nanowire, compatible with the geometry and the excitation scheme (an x-polarised plane wave.) In this section we identify the mode of operation of the antenna, we relate its propagation characteristics on the nanowire to the performance of the antennas, and we propose design models resting on modal results to predict the performance of the antennas.

4.1 Modal identification

The surface plasmon mode that is excited on the antennas must first be identified. To this end, we found the modes and their fields on a nanowire waveguide of the same cross-sectional configuration as one of the monopoles analysed in Sec. 3.1.1 (l = 210 nm, w = 20 nm, t = 40 nm). The wavelength for the modal analysis was set to $\lambda = \lambda_{res}$ = 2268 nm, which is the resonant wavelength of the aforementioned monopole. In order to remain consistent with the FDTD computations, the finite-difference mode solver in Lumerical was used and the same mesh as in the antenna cross-sectional plane (y-z plane, 0.5 nm mesh) was adopted. The same material properties for gold, silicon and water were retained.

Figures 18(a)-(b) show the real part of the transverse electric fields (which are at least 10× larger than their corresponding imaginary parts) and Fig. 18(c) shows the imaginary part of the longitudinal electric field (which is significantly larger than its real part) of the nanowire mode of interest computed using the mode solver. These field components are compared to the corresponding electric field components distributed over a y-z cross-section taken near the centre of the monopole antenna in Figs. 18(d)-(f) computed using the FDTD method. A very close resemblance between all corresponding field distributions is apparent from the results, suggesting that the mode of operation is correctly identified and that the antenna operates in only one surface plasmon mode (monomode operation). Based on the distribution of E_z we identify the mode as the sa_b^0 mode [18,19]. The longitudinal (E_x) field component of the monopole (Fig. 18(f)) has a large background level because it consists of the sum of the surface plasmon mode field and the incident (plane wave) field.

In general, the surface plasmon modes that are excited on an antenna depend on the polarisation and orientation of the source. Modes that share the same symmetry as the source, and that overlap spatially and in polarisation with the latter, can be excited.

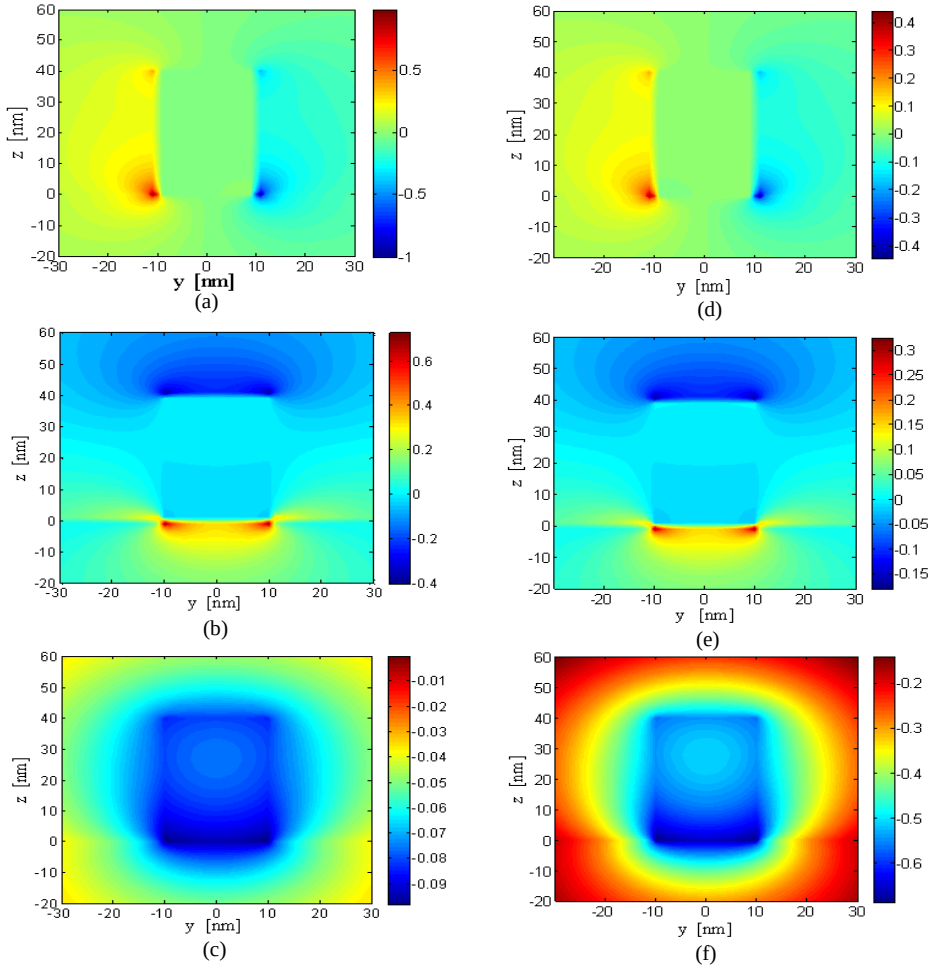

Fig. 18. (a)-(c) Electric field distribution of a surface plasmon mode plotted over the cross-section of a nanowire waveguide (w=20 nm, t=40 nm and λ_{res} = 2268 nm) computed using a mode solver. (d)-(f) Electric field distribution over a cross-section of the corresponding monopole antenna computed using the FDTD. (a) and (d) Re{E_y}, (b) and (e) Re{E_z}, (c) and (f) Im{E_x}.

4.2 Effective Index and Attenuation

Now that we have successfully identified the mode resonating in the monopoles, or each arm of the dipoles, we can evaluate the effective refractive index n_{eff} and the attenuation α of this mode as a function of the nanowire cross-section. For this purpose, the incident wavelength was arbitrarily fixed to λ_0=1400 nm and w and t were changed, one at the time, to determine their influence on n_{eff} and α. From these results we then explain some of the trends observed in the parametric study of Sec. 3.

Figures 19(a) and (b) give the computed results. Evidently, the effective index and the attenuation decrease with increasing nanowire width and thickness. Therefore, increasing the width or thickness of an antenna, while keeping its length fixed, results in a blue-shift of its resonant wavelength, because:

$$\lambda_{res} \propto n_{eff} \tag{4}$$

This behaviour is observed in our FDTD computations in Figs. 3 and 10, and in Figs. 4 and 13. It is worth noting here that the rate of change of n_{eff} and α decrease as w and t increase. Applying this observation to Eq. (4), we expect a smaller shift in the position of resonance as w and t increase. This is also observed in the trends of Figs. 3, 4, 10 and 13.

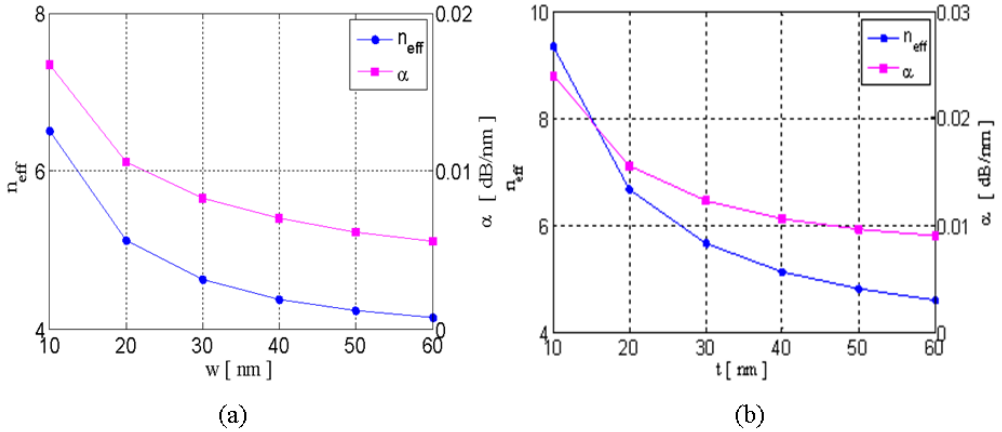

Fig. 19. Effective refractive index and attenuation of the mode resonating in the antennas as a function of (a) width using t=40 nm and (b) thickness using w= 20 nm, at λ=1400.

Next, w and t were fixed to representative values (w = 20 nm, t = 40 nm) and the incident wavelength was varied to determine its influence on n_{eff} and α. As is observed from Figs. 20(a) and (b), n_{eff} and α decrease with increasing wavelength. Returning to Figs. 16(c) and (d), for a fixed dipole arm length $d = (l - g)/2$, the FWHM decreases as w and t decrease because α decreases with the latter (recall that λ_{res} red-shifts with decreasing w and t - see Figs. 10 and 13 or the previous paragraph). However, if d varies, one needs to consider the product $d\alpha$ as the total loss. Given the slow rate of change of α with wavelength (Fig. 20 (b)), the total loss changes mostly with d. Increasing the length of the dipole while the gap is fixed thus increases the FWHM, as shown in Fig. 16(a) (d increases). However, increasing the gap while the antenna length is fixed decreases the FWHM, as shown Fig. 16(b) (d decreases). These observations also explain the results of Fig. 8 (broader response for smaller gaps).

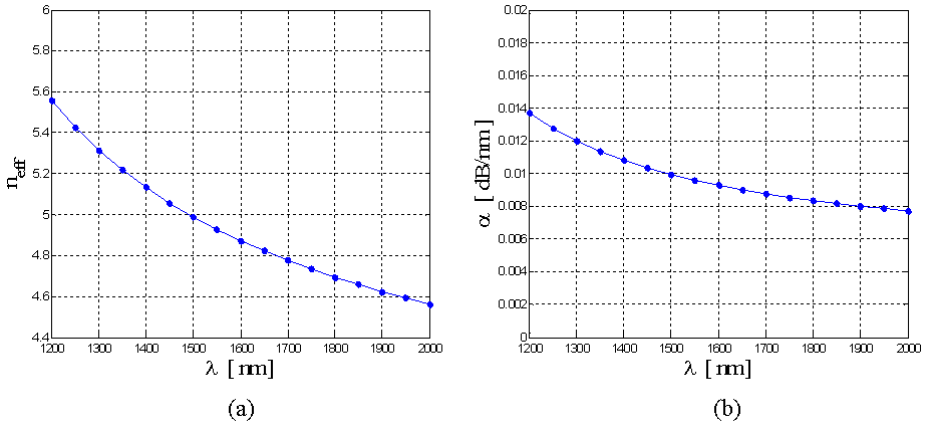

Fig. 20. (a) Effective index and (b) attenuation as a function of wavelength calculated from modal analysis for a nanowire waveguide of cross-section w = 20 nm by t =40 nm.

4.3 Effective Length of a Monopole Based on Modal Analysis

We wish to use the results of the modal analysis to estimate δ_a and the physical length l of the monopole required for resonance at a desired λ_{res}. An estimate, inspired from RF antenna theory, of the required physical length would be $l = \lambda_{res}/2n_{eff}$, where n_{eff} is obtained from modal analysis at the desired λ_{res}. However, this is incorrect because we know from the parametric study (section 3) that the monopole operation is such that it appears longer than its physical length due to fields extending beyond its ends (Fig. 17), *i.e.*, $L_{eff} > l$. We thus propose the following alternative relation:

$$\lambda_{res}=2L_{eff}n_{eff} \tag{5}$$

The nanowire of Sec. 4.1 (w = 20 nm, t = 40) was analysed at different wavelengths, corresponding to the resonance wavelengths λ_{res} of monopoles of length l (Fig. 2) in a pitch large enough to eliminate the coupling effects between neighboring monopoles (p=q=700 nm). (In fact, the values of n_{eff} were obtained from the data of Fig. 20 by interpolation at the required wavelengths). The decay of $|E_z|$ of the mode away from the nanowire along the z-axis was evaluated. In the positive z-direction (into the H_2O) $|E_z|$ falls to 1/e of its value a distance δ_w from the nanowire surface. In the negative z-direction (into the Si) $|E_z|$ falls to 1/e of its value a distance δ_s from the nanowire surface. The decays thus obtained from $|E_z|$ of the mode along with n_{eff} are summarised in Table 1. (In general $\delta_s \neq \delta_w$, in which case we would use a weighted decay length correction factor $\delta_m = (1-\tau)\delta_w + \tau\delta_s$, where $\tau/(1-\tau)$ is defined as the ratio of $|E_z|$ at the Au-Si interface to $|E_z|$ at the Au-H_2O interface.)

Table 1. Results of the Modal Analysis

	l (nm)	λ_{res} (nm)	n_{eff}	δ_w (nm)	δ_s (nm)	δ_m (nm)
1	90	1281	5.35	23	23	23
2	100	1358	5.20	24	24	24
3	110	1441	5.07	24	24	24
4	120	1526	4.96	25	25	25
5	130	1601	4.87	26	26	26

Substituting n_{eff} and λ_{res} corresponding to every value of physical length l from Table 1 into Eq. 5 yields L_{eff}. One can then estimate the physical length of the monopole l_{est} by analogy with Eq. (3) as:

$$l_{est} \approx L_{eff} - 2\delta_m \tag{6}$$

Using δ_m from Table 1, we find the estimated physical length of the monopoles l_{est} as summarised in Table 2. Our estimated lengths are all within 20% of the physical length, which is quite acceptable considering the relatively broad response of the monopoles. Part of this error may be caused by numerical inaccuracies due to the finite mesh size used in the FDTD and modal analyses.

Table 2. Estimated Lengths of Monopoles

	l_{est} (nm)	Error (%)
1	73.6	18
2	82.5	17.5
3	94	14.5
4	104	13
5	112	14

4.4 Transmission Line Model of Dipoles

A transmission line model with a lumped element as shown in Fig. 21 is proposed to account for the effect of the gap on the position of the resonant wavelength of dipoles observed in Fig.

8. In this model the gap is represented by capacitor C_g, which is connected to two open-circuited transmission lines, modelling the two arms of a dipole. $Z_{IN}^{(1)}$ and $Z_{IN}^{(2)}$ are the input impedances looking from the terminal port in Fig. 21, Z_0 is the characteristic impedance of the transmission lines, β is the propagation constant and $d + \delta_m$ is the length of each transmission line ($d = (l - g)/2$). β is taken as the phase constant of the mode resonating in the antenna (*i.e.*, based on n_{eff}, as computed in Sec. 4.2 near the expected resonance wavelength):

$$\beta = \omega\sqrt{\varepsilon_0\mu_0}/n_{eff}$$

Using a simple parallel-plate model, C_g is evaluated as

$$C_g = \varepsilon_{H_2O} A_d / g \tag{7}$$

where ε_{H_2O} is the permittivity of water, $A_d = wt$ is the cross-sectional area of the dipole arms, and g is the length of the gap.

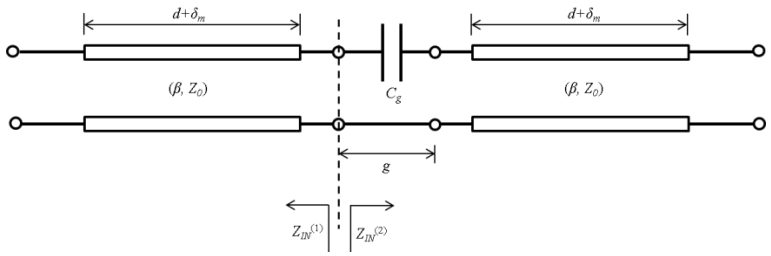

Fig. 21. Transmission line model of the dipole where the gap is modelled as a parallel-plate capacitor.

By Analogy to a lumped-element LC circuit, resonance occurs when the input impedances $Z_{IN}^{(1)}$ and $Z_{IN}^{(2)}$ add to zero [20]. For our model we have:

$$Z_{IN}^{(1)} = -jZ_0 \cot\big(\beta(d + \delta_m)\big) \tag{8.a}$$

$$Z_{IN}^{(2)} = \frac{-j}{\omega C_g} - jZ_0 \cot\big(\beta(d + \delta_m)\big) \tag{8.b}$$

which yields the following expression on resonance:

$$\tan\big(\omega_{res}\sqrt{\varepsilon_0\mu_0}(d + \delta_m)/n_{eff}\big) = -2\omega_{res}C_g Z_0 \tag{9}$$

where:

$$\omega_{res} = 2\pi c/\lambda_{res}$$

Solving Eq. (9) for λ_{res} (numerically) provides a good estimate to this wavelength without requiring time-consuming 3D FDTD modeling.

However, we must first determine the characteristic impedance Z_0 to be used. We assume Z_0 to be equal to the wave impedance Z_w of the mode, which is given in general as [21]:

$$Z_w = \frac{\hat{\boldsymbol{k}}\cdot(\boldsymbol{E}\times\boldsymbol{H}^*)}{(\hat{\boldsymbol{k}}\times\boldsymbol{H})\cdot(\hat{\boldsymbol{k}}\times\boldsymbol{H}^*)} \tag{10}$$

where the propagation direction is $\hat{\boldsymbol{k}} = \hat{\boldsymbol{x}}$ and $\boldsymbol{E}$ and $\boldsymbol{H}$ and are the modal electric and magnetic fields of the nanowire corresponding to the dipole of interest. Fig. 22 shows the real

part of Z_w over the y-z cross-section (w=20 nm, t=40 nm) of the nanowire, computed using Eq. (10). The nanowire waveguide has an inhomogeneous cross-section, so the mode does not have a unique Z_w. By averaging Z_w over a 300×300 nm^2 cross-section we obtain Z_w= 275 Ω. Note that the small region inside the metal where values of Z_w become large (z ~ 25 nm, y = 0) is due to the denominator of Eq. (10) becoming close to zero - Z_w is non-physical here so this region was removed from the averaging calculations.

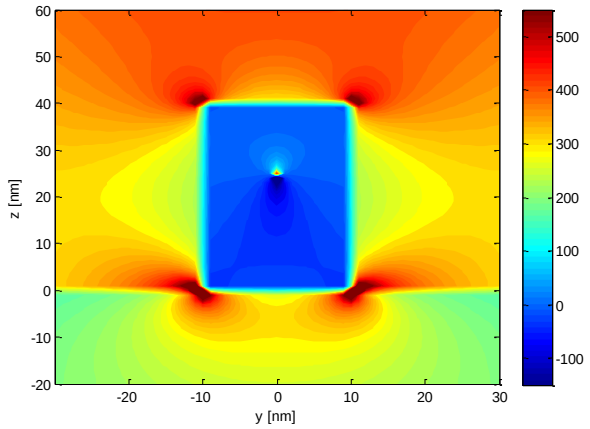

Fig. 22. Wave impedance over a y-z cross-section of the nanowire.

Going back to Eq. (9), we now solve for λ_{res} and plot the results in Fig. 23 as a function of gap length. We also plot the values obtained from the FDTD analysis of dipoles of l = 210 nm, w = 20 nm, t = 40 nm and variable gap lengths. The pitch was set to 700×700 nm^2 to eliminate coupling effects between antennas in the FDTD analysis, thus making the results directly comparable to the results of modal analysis. Very good agreement is noted.

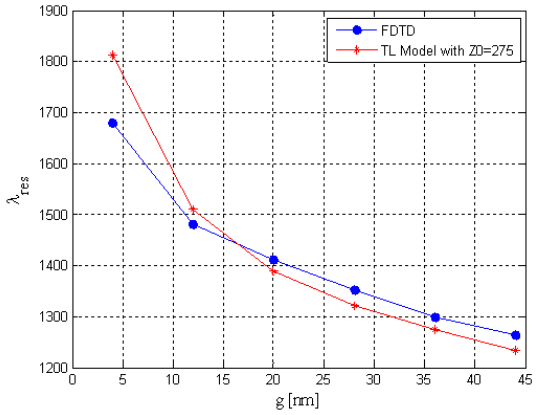

Fig. 23. λ_{res} obtained from FDTD analysis and from the transmission line model for a dipole of l= 210 nm, w= 20 nm, t= 40 nm and variable g.

5. Concluding Remarks

We performed a full parametric study of periodic plasmonic monopoles and dipoles in a piecewise homogeneous environment consisting of a silicon substrate and an aqueous cover. The study considered three system responses: transmittance, reflectance and absorptance. The responses were evaluated numerically and the results interpreted. Increasing the length red-shifts the resonance of monopoles and dipoles, whereas increasing the width, thickness and gap causes a blue-shift in their responses. We show that such trends are expected by

identifying the surface plasmon mode that is excited in the antennas (the sa_b^0 mode [18,19]) and computing its effective index and attenuation as a function of geometry and wavelength. The field enhancement ($|E_x|/|E_{inc}|$) and FWHM of dipoles were also computed, yielding values of up to ~100 in g = 4 nm gaps, and 30 to 40 THz, respectively.

We proposed an expression resting on modal results (for the surface plasmon mode excited in the antennas) to predict the resonant length of a monopole given its cross sectional dimensions and the required resonant wavelength. The expression, which takes into account field extension beyond the antenna ends, estimates the physical length of monopoles to within ~20% when compared with the FDTD results. Finally, we proposed a simple equivalent circuit, also resting on modal results, but involving transmission lines and a capacitor which models the gap, to determine the resonant wavelength of dipoles. This circuit successfully estimates the resonant wavelength of a dipole to within ~10% when compared to the FDTD results. The expression and the equivalent circuit should prove useful as design guidelines for optical monopole and dipole antennas.

2.4 Convergence Analysis

Convergence analysis was done by tracking the resonant wavelength of a nanoantenna for $dx=dy=dz$=0.25, 0.5, 1, and 2 nm, where dx, dy, and dz are the dimension of mesh cells around the antenna. The results are shown in Fig. 3, as well as the expected convergence value at zero, calculated using Richardson Extrapolation Formula. The 0.5×0.5×0.5 nm^3 mesh that is used throughout this study gives 2.1% numerical error.

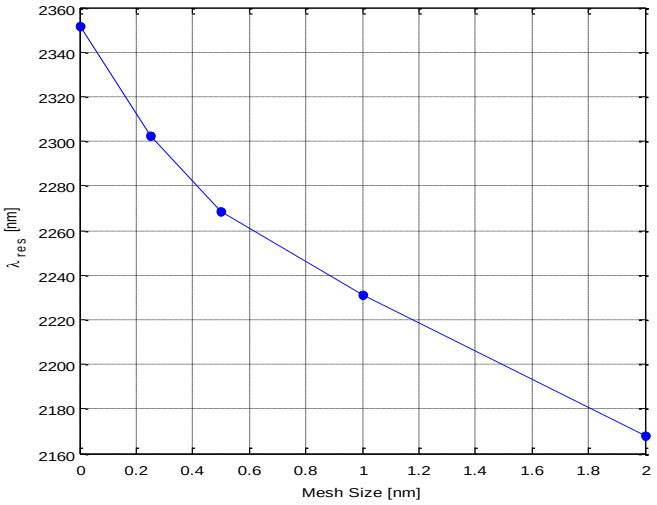

Fig. 3. Convergence results

2.5 Effects of Pitch

Changing the pitch, while keeping antenna length and width constant varies the coupling between adjacent antennas and hence the response of the system. Figs. 4 and 5 show the system response as a function of square and non-square pitch, respectively. For a square pitch, where $p=q$, a slight blue-shift, followed by a red-shift can be seen in the system response as p and q increase. At $p=q$=400 and 450 nm the response of the system is not as smooth as it is for smaller pitch. This issue, as well as the trends of the system response as a function of pitch need to be further investigated.

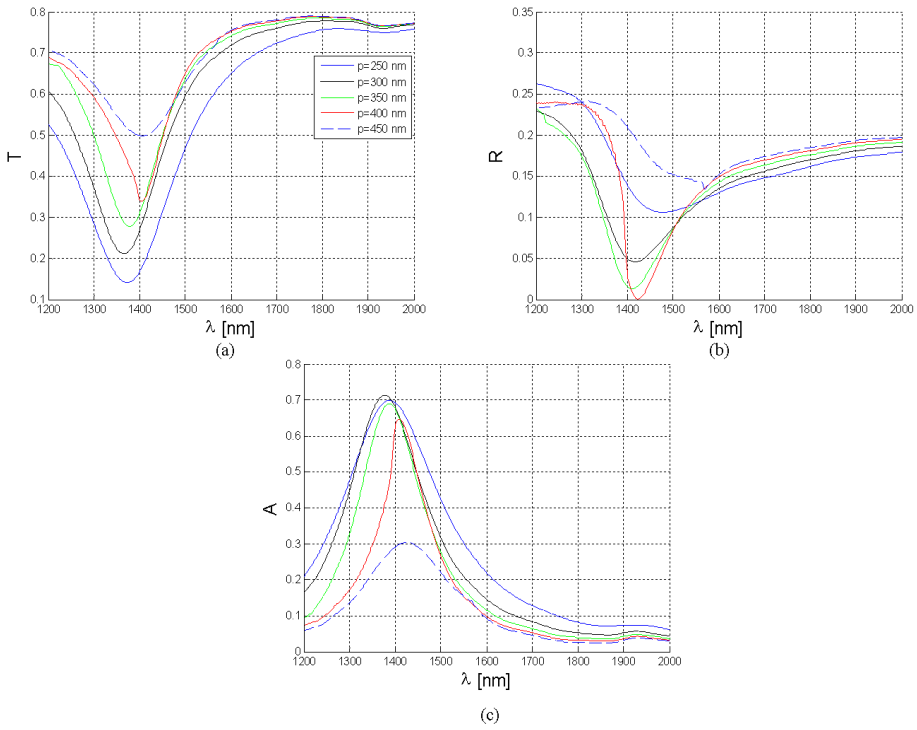

Fig. 4.(a) Transmittance, (b) reflectance and (c) absorptance versus wavelength for dipole antennas of *l*=210 nm, g=20 nm, *w*=20 nm, *t*=40 nm and variable *p*=*q*(given in legend inset to (a)).

For a non-square pitch, where *p*=300 nm and *q* varies from 150 to 350 nm, as shown in Fig.5, a red-shift is clear in T, R and A. Further investigation is required to determine the cause of this red-shift.

Considering the FWHM of the system response, as well as the level of absorptance at *p*=*q*=300 nm, a relatively narrow response with high level of absorptance is observed. Thus 300 nm was chosen as the cell dimensions throughout this study.

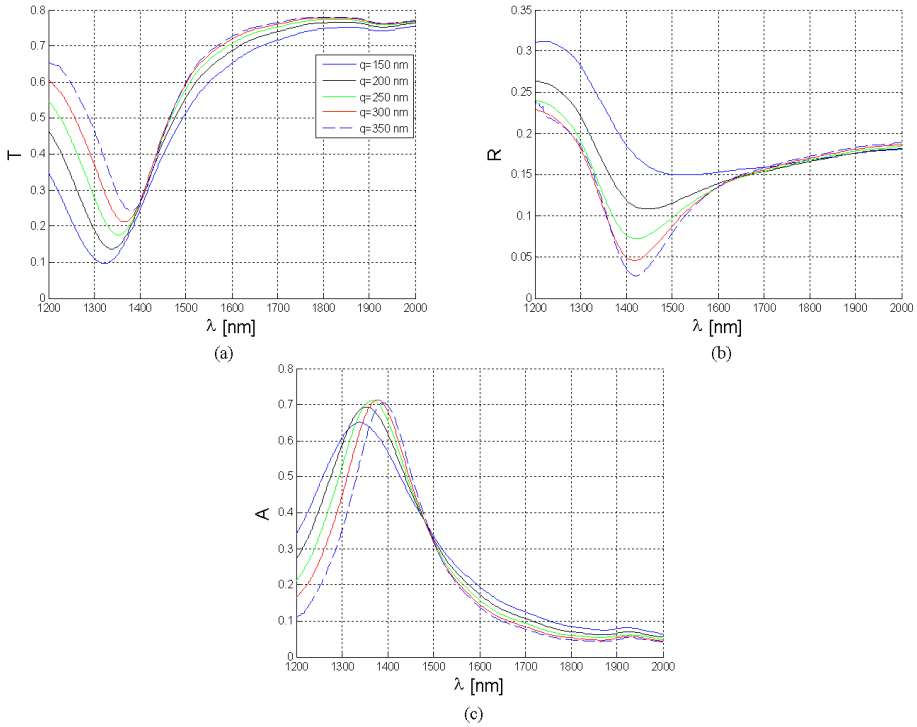

Fig. 5.(a) Transmittance, (b) reflectance and (c) absorptance versus wavelength for dipole antennas of *l*=210 nm, g=20 nm, *w*=20 nm, *t*=40 nm, *p*=300 nm, and variable *q* (given in legend inset to (a)).

Chapter 3

Conclusions

3.1 Summary and Thesis Contributions

Periodic gold nanoantennas on silicon and covered by water were considered and analysed numerically and theoretically. A full parametric study of the response of the system was done through 3D FDTD simulations. The resultant trends were determined and interpreted physically. The plasmonic mode resonating in nanomonopoles was identified by comparing the electric field distributions over a yz cross-section of a nanomonopole illuminated by a plane wave in FDTD analysis to the distribution of the modal electric fields of an infinitely long plasmonic waveguide of the same cross-sectional dimensions. Effective refractive index and loss of the plasmonic mode were evaluated as a function of the incident wavelength, as well as the width and thickness of the waveguide.

A theoretical model, which can easily estimate the resonant length of a nanomonopole was proposed. In this model the decay length of the transverse modal fields was used as a scaling factor. A transmission line model was also developed to estimate the resonant length of nanodipoles, in which the gap is modeled as a parallel plate capacitor, connected in series with the two arms of the dipole, modeled as two transmission lines. This model can predict the resonant wavelength of nanodipoles to within a 10% error with respect to rigorous 3D FDTD analysis. The length of the transmission lines can be estimated by the model proposed for determining the resonant length of nanomonopoles.

3.2 Suggestions for Future Work

Experimental work is required to confirm the numerical results obtained. Designs need to be further optimized in terms of bulk and surface sensitivities to get the best response for the intended application. Achieving sharp and intense responses by adjusting the antenna parameters would result in better detection of the spectral response of the system in the experimental work. The array factor could be analysed as another design parameter, which may have a significant effect on the intensity of response. It may be worthwhile to look at different antenna designs to achieve higher order resonances, as well as the Fano resonance.

Biblography

1. P. Bharadwaj, B. Deutsch, L. Novotny, "Optical antennas," Advances in Optics and Photonics **1,** 438-483 (2009).
2. N. W.Ashcroftand N. D. Mermin, *Solid State Physics*, (Brooks Cole, 1976).
3. W. Rechberger, A. Hohenau, A. Leitner, JR. Krenn, B. Lamprecht, F.R. Aussenegg, "Optical properties of two interacting gold nanoparticles,"Opt. Comm. **220**, 137-141 (2003).
4. K. L. Kelly, E. Coronado, L. L. Zhao, and G. C. Schatz, "The optical properties of metal nanoparticles: the influence of size, shape, and dielectric environment," J. Phys. Chem. B **107**, 668-677 (2003).
5. S. Kuhn, U. Hakanson, L. Rogobete, and V. Sandoghdar, "Enhancement of single-molecule fluorescence using a gold nanoparticle as an optical nanoantenna," Phys. Rev. Lett.**97,** 017402 (2006).
6. G. W. Bryant, F. J. Garcia de Abajo, J. Aizpurua, "Mapping the plasmon resonance of metalic nanoantennas," Nano Lett. **8**, 631-636 (2008).
7. J. Dorfmuller, R.Vogelgesang,W.Khunsin, C.Rockstuhl,C.Etrich, and K. Kern, "Plasmonic nanowire antennas: experiment, simulation, and theory," Nano Lett.**10,** 3596-3603 (2010).
8. E. J. Smythe, E. Cubukcu, and F.Capasso, "Optical properties of surface plasmon resonances of coupled metallic nanorods," Opt. Express **15**, 7439-7447 (2007)
9. A.Rashidi, H.Mosallaei, and R.Mittra, "Scattering analysis of plasmonic nanorods antennas: A novel numerically efficient computational scheme utilizing macro basis functions," J. Appl. Phys.**109**, 123109 (2011)
10. A. Pors, M. Willatzen, O. Albrektsen, and Sergey I. Bozhevolnyi, "From plasmonic nanoantennas to split-ring resonators: tuning scattering strength," J. Opt. Soc. Am. B**27,** 1680-1687 (2010).
11. W. Ding, R. Bachelot, S. Kostcheev, P. Royer, R. Espiau de Lamaestre, "Surface plasmon resonances in silver Bowtie nanoantennas with varied bow angles," J. Appl. Phys. **108**, 124314 (2010).
12. T. Lin, S. Chang, S. L. Chuang, Z. Zhang, andP. J.Schuck, "Coating effect on optical resonance of plasmonic nanobowtie antenna," Appl. Phys. Lett.**97**, 063106 (2010).
13. N. A. Hatab, C.Hsueh, A. L. Gaddis, S. T. Retterer, J.Li,G.Eres, Z. Zhang, and B.Gu,"Free-standing optical gold bowtie nanoantenna with variable gap size for enhanced Raman spectroscopy," Nano Lett. **10,** 4952–4955 (2010).
14. A. Kinkhabwala, Z. Yu, S. Fan, Y. Avlasevich, K Mullen and W. E. Moerner, "Large single-molecule fluorescence enhancements produced by a bowtie nanoantenna," Nature Photonics **3,** 654-657 (2009).

15. J. N. Farahani, H. Eisler, D. W. Pohl, M. Pavius, P. Fluckiger, P. Gasser and B. Hecht, "Bow-tie optical antenna probes for single-emitter scanning near-field optical microscopy," Nanotechnology **18,** 125506 (2007).

16. H. Fischer and O. J. F. Martin, "Engineering the optical response of plasmonic nanoantennas," Opt. Express **16**, 9144-9154 (2008).

17. F. P. Garcia de Arquer, V. Volski, N. Verellen, G. A. E. Vandenbosch, and V. V. Moshchalkov, "Engineering the input impedance of optical nano dipole antennas: material, geometry and excitation effect,"IEEE Trans. Antennas Propag. **59,** 3144-3153 (2011).

18. L. Novotny, "Effective wavelength scaling for optical antennas," Phys. Rev. Lett.**98**, 266802 (2007).

19. W. Ding, R. Bachelot, R. Espiau de Lamaestre, D. Macias, A.-L.Baudrion, P. Royer, "Understanding near/far-field engineering of optical dimer antennas through geometry modification," Opt. Express **17**, 21228-21239 (2009).

20. E. Cubukcu and F. Capasso, "Optical nanorod antennas as dispersive one-dimensional Fabry-Perot resonators for surface plasmons," Appl. Phys. Lett.**95**, 201101 (2009).

21. A. Alú and N. Engheta, "Tuning the scattering response of optical nanoantennas with nanocircuit loads," Nature Photonics **2**, 307-310, (2008).

22. P. Biagioni, M. Savoini, J. Huang, L. Duó, M. Finazzi, B. Hecht, "Near-field polarization shaping by a near-resonant plasmonic cross antenna," Phys. Rev. B **80**, 153409 (2009).

23. N. Verellen, P. V. Dorpe, C. Huang, K. Lodewijks, G. A. E. Vandenbosch, L. Lagae, V. V. Moshchalkov, "Plasmon Line Shaping Using Nanocrosses for High Sensitivity Localized Surface Plasmon Resonance Sensing," Nano Lett. **11**, 391–397 (2011).

24. L. Tang, S. E. Kocabas, S. Latif, A. K. Okyay, D. S. L. Gagnon, K. C. Saraswat, D. A. B. Miller, "Nanometer-scale germanium photodetector enhanced by a near-infrared dipole antenna," Nature Photonics **2**, 226-229 (2008).

25. J. P. Kottmann and O. J. F. Martin, "Retardation-induced plasmon resonances in coupled nanoparticles," Opt. Lett. **26,** 1096-1098 (2001).

26. P.Biagioni, J. Huang, and B. Hecht, "Nanoantennas for visible and infrared radiation," Rep. Prog.Phys. **75,** 024402(2012).

27. P. Berini and R. Buckley, "On the convergence and accuracy of numerical mode computations of surface plasmon waveguides," J. Comput.Theor.Nanosci**6,** 2040-2053 (2009).

28. C. Chen and P. Berini, "Grating couplers for broadside input and output coupling of long-range surface plasmons," Opt. Express **18,** 8006-8018 (2010).

29. P. Berini, "Plasmon-polariton waves guided by thin lossy metal films of finite width: bound modes of symmetric structures," Phys. Rev. B **61,** 10484-10503 (2000).

30. T. H. Taminiau, F. D. Stefani, and N. F. van Hulst, "Enhanced directional excitation and emission of single emitters by a nano-optical Yagi-Uda antenna," Opt. Express **16,** 16858-16866 (2008).